

# Radiative and Electroweak Penguin Decays of $B$ Mesons

TOBIAS HURTH

*Inst. for Physics, Johannes Gutenberg University, D-55099 Mainz, Germany;*  
*email: Tobias.Hurth@cern.ch*

AND MIKIHICO NAKAO

*KEK, High Energy Accelerator Research Organization, Tsukuba, 305-0801,*  
*Japan and the Graduate University for Advanced Studies (Sokendai), Tsukuba,*  
*305-0801, Japan; email: mikihiro.nakao@kek.jp*

**Abstract** The huge datasets collected at the two  $B$  factories, Belle and BaBar, have made it possible to explore the radiative penguin process  $b \rightarrow s\gamma$ , the electroweak penguin process  $b \rightarrow s\ell^+\ell^-$  and the suppressed radiative process  $b \rightarrow d\gamma$  in detail, all in exclusive channels and inclusive measurements. Theoretical tools have also advanced to meet or surpass the experimental precision, especially in inclusive calculations and the various ratios of exclusive channels. In this article, we review the theoretical and experimental progress over the past decade in the radiative and electroweak penguin decays of  $B$  mesons.

## CONTENTS

INTRODUCTION . . . . .	2
THEORETICAL FRAMEWORK . . . . .	3
<i>Electroweak Effective Hamiltonian</i> . . . . .	4
<i>Perturbative Corrections to Inclusive Decays</i> . . . . .	5
<i>Hadronic Power Corrections to Inclusive Modes</i> . . . . .	9
<i>Nonperturbative Corrections due to Kinematical Cuts</i> . . . . .	12
<i>Charmonium Resonance Contributions</i> . . . . .	13
<i>Soft Collinear Effective Theory for Exclusive Decays</i> . . . . .	13
EXPERIMENTAL TECHNIQUES . . . . .	16
<i>Exclusive <math>B</math> Reconstruction</i> . . . . .	16
<i>Inclusive Measurement Techniques</i> . . . . .	16
PRESENT THEORETICAL PREDICTIONS . . . . .	17
<i>Inclusive Penguin Decays</i> . . . . .	17
<i>Exclusive Penguin Decays</i> . . . . .	20
PRESENT EXPERIMENTAL RESULTS . . . . .	24
<i>Inclusive <math>B \rightarrow X_s\gamma</math> Branching Fraction</i> . . . . .	24
<i>Exclusive Measurements of <math>b \rightarrow s\gamma</math> Processes</i> . . . . .	24
<i><math>CP</math> and Isospin Asymmetries in <math>b \rightarrow s\gamma</math> Processes</i> . . . . .	25

<i>Measurements of <math>b \rightarrow d\gamma</math> Processes</i> . . . . .	26
<i>Exclusive <math>B \rightarrow K^{(*)}\ell^+\ell^-</math> Branching Fraction</i> . . . . .	28
<i><math>B \rightarrow K^{(*)}\ell^+\ell^-</math> Asymmetries and Angular Distributions</i> . . . . .	28
<i>Inclusive <math>B \rightarrow X_s\ell^+\ell^-</math> Branching Fraction</i> . . . . .	29
OUTLOOK . . . . .	29

## 1 INTRODUCTION

The  $B$  meson system, which is a bound state that consists of a  $b$  quark and a light antiquark, provides an ideal laboratory for precise study of the Standard Model (SM) of particle physics, and thus facilitates the search for new physics (NP). Because the  $b$  quark mass is much larger than the typical scale of the strong interaction, the otherwise troublesome long-distance strong interactions are generally less important and are under better control than in other lighter meson systems. Radiative penguin<sup>1</sup> decays of the  $B$  meson with the emission of a photon ( $\gamma$ ) and electroweak penguin decays with the emission of a lepton pair ( $\ell^+\ell^-$ ,  $\ell = e, \mu$ ) are of particular interest in this respect. These processes reveal the flavor changing neutral current (FCNC), that is the transition of a  $b$  quark with an electric charge of  $-1/3$  into an  $s$  or a  $d$  quark of the same charge. In the SM, the FCNC occurs only via virtual loop diagrams (Fig. 1). Additional NP contributions to these decay rates are not necessarily suppressed with respect to the SM contribution. Examples of such NP scenarios include those in which the SM particles in the loop diagram are replaced by hypothetical new particles at a high mass scale; so far, they have not been directly accessible in collider experiments. Radiative and electroweak penguin decays are highly sensitive to NP because they are theoretically well-understood and have been extensively measured at the  $B$  factories. The search for such NP effects complements the search for new particles produced at collider experiments.

The first generation of the  $B$  factories at KEK (the Belle experiment at the KEKB  $e^+e^-$  collider) (3) and at SLAC (the BaBar experiment at the PEP-II  $e^+e^-$  collider) (4) have collected huge samples of  $B$  meson decays and have thereby established the SM picture of  $CP$  violation and other flavor-changing processes in the quark sector. These processes are governed by a single  $3 \times 3$  unitarity matrix referred to as the Cabibbo-Kobayashi-Maskawa (CKM) matrix (5,6). The CKM matrix can be illustrated by a unitarity triangle in the complex plane that is overconstrained by measurements from the  $B$  factories, the Tevatron  $B$  physics programs (namely the CDF (7) and D0 (8) experiments), and earlier kaon decay experiments. In other words, none of the current measurements of  $B$  meson decays have observed any unambiguous sign of NP (9,10). Although this experimental result is an impressive success of the CKM theory within the SM, there is still room for sizable new effects from new flavor structures, given that FCNC processes have been tested up to only the 10% level.

The nonexistence of large NP effects in the FCNC processes hints at the famous flavor problem, namely why FCNCs are suppressed. This problem must be solved in any viable NP model. Either the mass scale of the new degrees of freedom is very high or the new flavor-violating couplings are small for reasons that remain to be found. For example, assuming generic new flavor-violating couplings, the

---

<sup>1</sup>The name penguin decays was first introduced in Ref. (1) as the result of a bet. A more detailed account of the name can be found in Ref. (2).

present data on  $K$ - $\bar{K}$  mixing implies a very high NP scale of order  $10^3$ – $10^4$  TeV depending on whether the new contributions enter at loop-level or at tree-level. In contrast, theoretical considerations on the Higgs sector, which is responsible for the mass generation of the fundamental particles in the SM, call for NP at order 1 TeV. As a consequence, any NP below the 1-TeV scale must have a nongeneric flavor structure. The present measurements of  $B$  decays, especially of FCNC processes, already significantly restrict the parameter space of NP models. For further considerations on NP, the reader is referred to another article in this volume (11) and to Ref. (12).

Quark-level FCNC processes such as  $b \rightarrow s\gamma$ , to which NP may contribute, cannot be directly measured because the strong interaction forms hadrons from the underlying quarks. Instead, the experimentally measured and theoretically calculated process is a  $B$  meson decay into a photon plus an inclusive hadronic final state  $X_s$ , which includes all the hadron combinations that carry the strange quantum number  $s = +1$  of the  $s$  quark.<sup>2</sup> Exclusive final states with one or a few specific hadrons in the final state (e.g.,  $B \rightarrow K^*\gamma$ ) have less predictive power theoretically; however, because the measurements are easier and better defined, there are other useful observables beyond branching fractions, in particular  $CP$ , forward-backward, isospin, and polarization asymmetries. In the future, a large overconstrained set of measurements of these observables will allow us to detect specific patterns and to distinguish between various NP scenarios.

This review covers progress in radiative and electroweak decays in the past decade, during which a huge number of  $B$  factory results were accumulated and significant progress in various theoretical aspects was achieved. The pioneering work that led to the first observation of the  $b \rightarrow s\gamma$  process by CLEO (13, 14) was discussed in an earlier volume of this journal (15).

Our review is organized as follows. In Section 2, we describe theoretical tools for radiative and electroweak penguin decays, and in Section 3 we describe experimental techniques. We give theoretical predictions in Section 4 and summarize the measurements of radiative and electroweak penguin decays in Section 5. Finally, we briefly discuss future prospects in Section 6.

## 2 THEORETICAL FRAMEWORK

Inclusive  $B$  decays are theoretically clean because they are dominated by partonic (perturbatively calculable) contributions. Nonperturbative corrections are in general rather small (16, 17, 18). This result can be derived with the help of the heavy mass expansion (HME) of the inclusive decay rates in inverse powers of the  $b$  quark mass. Up-to-date predictions of exclusive  $B$  decays are based on the quantum chromodynamics (QCD)-improved factorization (QCDF) and soft collinear effective theory (SCET) methods. In general, exclusive modes have larger nonperturbative QCD corrections than do inclusive modes.

---

<sup>2</sup>In this review, we use the following notations and conventions: We denote the inclusive decay as  $B \rightarrow X_s\gamma$  when charge conjugation is implied, or as  $\bar{B} \rightarrow X_s\gamma$  and  $B \rightarrow X_{\bar{s}}\gamma$  to reflect the quark charges of the underlying processes  $b \rightarrow s\gamma$  and  $\bar{b} \rightarrow \bar{s}\gamma$ , respectively, when  $CP$  and angular asymmetries are concerned. Here,  $B$  denotes either an isospin- and  $CP$ -averaged state of  $B^0$ ,  $\bar{B}^0$ ,  $B^+$  and  $B^-$  mesons, or an isospin averaged state of  $B^0$  and  $B^+$  (in the latter case,  $\bar{B}$  denotes  $\bar{B}^0$  and  $B^-$ ). Expressions are constructed similarly for inclusive  $X_d\gamma$  and  $X_s\ell^+\ell^-$  final states, and isospin-averaged exclusive final states. In the literature, the notation  $\bar{B} \rightarrow X_s\gamma$  is also commonly used for the case that includes charge conjugation.

## 2.1 Electroweak Effective Hamiltonian

Rare  $B$  decays are governed by an interplay between the weak and strong interactions. The QCD corrections that arise from hard gluon exchange bring in large logarithms of the form  $\alpha_s^n(m_b) \log^m(m_b/M)$ , where  $M = m_t$  or  $M = m_W$  and  $m \leq n$  (with  $n = 0, 1, 2, \dots$ ). These large logarithms are a natural feature in any process in which two different mass scales are present. To obtain a reasonable result, one must resum at least the leading-log (LL) series,  $n = m$ , with the help of renormalization-group techniques. Working to next-to-leading-log (NLL) or next-to-next-to-leading-log (NNLL) precision means that one resums all the terms with  $n = m + 1$  or  $n = m + 2$ . A suitable framework in which to achieve the necessary resummations of the large logarithms is an effective low-energy theory with five quarks; this framework is obtained by integrating out the heavy particles, which in the SM are the electroweak bosons and the top quark.

This effective field theory approach serves as a theoretical framework for both inclusive and exclusive modes. The standard method of the operator product expansion (OPE) (19,20) allows for a separation of the  $B$  meson decay amplitude into two distinct parts: the long-distance contributions contained in the operator matrix elements and the short-distance physics described by the so-called Wilson coefficients.

The electroweak effective Hamiltonian (21, 22, 23) can be written as

$$\mathcal{H}_{\text{eff}} = \frac{4G_F}{\sqrt{2}} \sum C_i(\mu, M) \mathcal{O}_i(\mu), \quad (1)$$

where  $\mathcal{O}_i(\mu)$  are the relevant operators and  $C_i(\mu, M)$  are the corresponding Wilson coefficients. As the heavy fields are integrated out, the complete top and  $W$  mass dependence is contained in the Wilson coefficients. Clearly, only within the observable  $\mathcal{H}_{\text{eff}}$  does the scale dependence cancel out.  $G_F$  denotes the Fermi coupling constant.

From the  $\mu$  independence of the effective Hamiltonian, one can derive a renormalization group equation (RGE) for the Wilson coefficients  $C_i(\mu)$ :

$$\mu \frac{d}{d\mu} C_i(\mu) = \gamma_{ji} C_j(\mu), \quad (2)$$

where the matrix  $\gamma$  is the anomalous dimension matrix of the operators  $\mathcal{O}_i$ , which describes the anomalous scaling of the operators with respect to the scaling at the classical level. At leading order, the solution is given by

$$\tilde{C}_i(\mu) = \left[ \frac{\alpha_s(\mu_W)}{\alpha_s(\mu)} \right]^{\frac{\tilde{\gamma}_{ii}^0}{2\beta_0}} \tilde{C}_i(\mu_W) = \left[ \frac{1}{1 + \beta_0 \frac{\alpha_s(\mu)}{4\pi} \ln \frac{\mu_W^2}{\mu^2}} \right]^{\frac{\tilde{\gamma}_{ii}^0}{2\beta_0}} \tilde{C}_i(\mu_W), \quad (3)$$

where  $\mu d/d\mu \alpha_s = -2\beta_0 \alpha_s^2/(4\pi)$ , and  $\beta_0$  and  $\tilde{\gamma}_{ii}^0$  correspond to the leading anomalous dimensions of the coupling constant and of the operators, respectively. The tilde indicates that the diagonalized anomalous dimension matrix is used.

Although the Wilson coefficients  $C_i(\mu)$  enter both inclusive and exclusive processes and can be calculated with perturbative methods, the calculational approaches to the matrix elements of the operators differ between the two cases. Within inclusive modes, one can use the quark-hadron duality to derive a well-defined HME of the decay rates in powers of  $\Lambda/m_b$  (24, 25, 26, 27, 28, 29). In

particular, the decay width of the  $B \rightarrow X_s \gamma$  is well approximated by the partonic decay rate, which can be calculated in renormalization-group-improved perturbation theory (30, 31):

$$\Gamma(B \rightarrow X_s \gamma) = \Gamma(b \rightarrow X_s^{\text{parton}} \gamma) + \Delta^{\text{nonpert.}}. \quad (4)$$

In exclusive processes, however, one cannot rely on quark-hadron duality, so one must estimate the matrix elements between meson states. A promising approach is the QCDF-method, which has been systematized for nonleptonic decays in the heavy quark limit (32, 33, 34). In addition, a more general quantum field theoretical framework for QCDF, known as SCET, has been proposed (35, 36, 37, 38, 39, 40). This method allows for a perturbative calculation of QCD corrections to naïve factorization and is the basis for the up-to-date predictions for exclusive rare  $B$  decays. However, within this approach, a general quantitative method to estimate the important  $\Lambda/m_b$  corrections to the heavy quark limit is missing.

## 2.2 Perturbative Corrections to Inclusive Decays

Within inclusive  $B$  decay modes, short-distance QCD effects are very important. For example, in the  $B \rightarrow X_s \gamma$  decay these effects lead to a rate enhancement by a factor of greater than two. Such effects are induced by hard-gluon exchanges between the quark lines of the one-loop electroweak diagrams. The corresponding large logarithms have to be summed as discussed above.

The effective electroweak Hamiltonian that is relevant to  $b \rightarrow s/d \gamma$  and  $b \rightarrow s/d \ell^+ \ell^-$  transitions in the SM reads

$$\mathcal{H}_{\text{eff}} = -\frac{4G_F}{\sqrt{2}} \left[ \lambda_q^t \sum_{i=1}^{10} C_i \mathcal{O}_i + \lambda_q^u \sum_{i=1}^2 C_i (\mathcal{O}_i - \mathcal{O}_i^u) \right], \quad (5)$$

where the explicit CKM factors are  $\lambda_q^t = V_{tb} V_{tq}^*$  and  $\lambda_q^u = V_{ub} V_{uq}^*$ . The unitarity relations  $\lambda_q^c = -\lambda_q^t - \lambda_q^u$  have already been used. The dimension-six operators are

$$\begin{aligned} \mathcal{O}_1 &= (\bar{s}_L \gamma_\mu T^a c_L) (\bar{c}_L \gamma^\mu T^a b_L), & \mathcal{O}_2 &= (\bar{s}_L \gamma_\mu c_L) (\bar{c}_L \gamma^\mu b_L), \\ \mathcal{O}_1^u &= (\bar{s}_L \gamma_\mu T^a u_L) (\bar{u}_L \gamma^\mu T^a b_L), & \mathcal{O}_2^u &= (\bar{s}_L \gamma_\mu u_L) (\bar{u}_L \gamma^\mu b_L), \\ \mathcal{O}_3 &= (\bar{s}_L \gamma_\mu b_L) \sum_q (\bar{q} \gamma^\mu q), & \mathcal{O}_4 &= (\bar{s}_L \gamma_\mu T^a b_L) \sum_q (\bar{q} \gamma^\mu T^a q), \\ \mathcal{O}_5 &= (\bar{s}_L \Gamma b_L) \sum_q (\bar{q} \Gamma' q), & \mathcal{O}_6 &= (\bar{s}_L \Gamma T^a b_L) \sum_q (\bar{q} \Gamma' T^a q), \\ \mathcal{O}_7 &= \frac{e}{16\pi^2} m_b (\bar{s}_L \sigma^{\mu\nu} b_R) F_{\mu\nu}, & \mathcal{O}_8 &= \frac{g_s}{16\pi^2} m_b (\bar{s}_L \sigma^{\mu\nu} T^a b_R) G_{\mu\nu}^a, \\ \mathcal{O}_9 &= \frac{e^2}{16\pi^2} (\bar{s}_L \gamma_\mu b_L) \sum_\ell (\bar{\ell} \gamma^\mu \ell), & \mathcal{O}_{10} &= \frac{e^2}{16\pi^2} (\bar{s}_L \gamma_\mu b_L) \sum_\ell (\bar{\ell} \gamma^\mu \gamma_5 \ell), \end{aligned} \quad (6)$$

where  $\Gamma = \gamma_\mu \gamma_\nu \gamma_\lambda$  and  $\Gamma' = \gamma^\mu \gamma^\nu \gamma^\lambda$ . The subscripts  $L$  and  $R$  refer to left- and right-handed components, respectively, of the fermion fields. In  $b \rightarrow s$  transitions the contributions proportional to  $\lambda_s^u$  are rather small, whereas in  $b \rightarrow d$  decays, where  $\lambda_d^u$  is of the same order as  $\lambda_d^t$ ; these contributions play an important role in  $CP$  and isospin asymmetries. The semileptonic operators  $\mathcal{O}_9$  and  $\mathcal{O}_{10}$  occur only in the semileptonic  $b \rightarrow s/d \ell^+ \ell^-$  modes.

Among the four-quark operators, only the effective couplings for  $i = 1, 2$  are large at the low scale  $\mu = m_b$  [ $C_{1,2}(m_b) \sim 1$ ], whereas the couplings of the other four-quark operators have almost negligible values. But the dipole operators [ $C_7(m_b) \sim -0.3$ ,  $C_8(m_b) \sim -0.15$ ] and the semileptonic operators [ $C_9(m_b) \sim 4$ ,  $C_{10}(m_b) \sim -4$ ] also play a significant role.

There are three principal calculational steps that lead to the LL (NNLL) result within the effective field theory approach:

1. The full SM theory must be matched with the effective theory at the scale  $\mu = \mu_W$ , where  $\mu_W$  denotes a scale of order  $m_W$  or  $m_t$ . The Wilson coefficients  $C_i(\mu_W)$  pick up only small QCD corrections, which can be calculated within fixed-order perturbation theory. In the LL (NNLL) program, the matching has to be worked out at the  $O(\alpha_s^0)$  [ $O(\alpha_s^2)$ ] level.
2. The evolution of these Wilson coefficients from  $\mu = \mu_W$  down to  $\mu = \mu_b$  must then be performed with the help of the renormalization group, where  $\mu_b$  is of the order of  $m_b$ . As the matrix elements of the operators evaluated at the low scale  $\mu_b$  are free of large logarithms, the latter are contained in resummed form in the Wilson coefficients. For the LL (NNLL) calculation, this RGE step has to be performed using the anomalous-dimension matrix up to order  $\alpha_s^1$  ( $\alpha_s^3$ ).
3. To LL (NNLL) precision, the corrections to the matrix elements of the operators  $\langle s\gamma | \mathcal{O}_i(\mu) | b \rangle$  at the scale  $\mu = \mu_b$  must be calculated to order  $\alpha_s^0$  ( $\alpha_s^2$ ) precision. The calculation also includes bremsstrahlung corrections.

**$B \rightarrow X_s \gamma$**  The error of the LL prediction of the  $B \rightarrow X_s \gamma$  branching fraction (41, 42, 43, 44) is dominated by a large renormalization scale dependence at the  $\pm 25\%$  level, which indicates the importance of the NLL series. By convention, the dependence on the renormalization scale  $\mu_b$  is obtained by the variation  $m_b/2 < \mu_b < 2m_b$ . The three calculational steps of the NLL enterprise—Step 1 (45, 46), Step 2 (47, 48), and Step 3 (49, 50, 51, 52, 53)—have been performed by many different groups and have been independently checked. The resulting NLL prediction had a small dependence on the scale  $\mu_b$  as well as on the matching scale  $\mu_0$  below 5%. But as first observed in Ref. (54), there was a large charm mass-scheme dependence because the charm loop vanishes at the LL level and the significant charm dependence begins only at the NLL level. By varying  $m_c/m_b$  in the conservative range  $0.18 \leq m_c/m_b \leq 0.31$ , which covers both the pole mass value (with its numerical error) and the running mass value  $\overline{m}_c(\mu_c)$  with  $\mu_c \in [m_c, m_b]$ , one finds an uncertainty of almost 10% (55, 56). This uncertainty is the dominant error in the NLL prediction. The renormalization scheme for  $m_c$  is an NNLL issue, and a complete NNLL calculation reduces this large uncertainty by at least a factor of two (57). This finding motivated the NNLL calculation of the  $B \rightarrow X_s \gamma$  branching fraction.

Following a global effort, such an NNLL calculation was recently performed and led to the first NNLL prediction of the  $B \rightarrow X_s \gamma$  branching fraction (58). This result is based on various highly-nontrivial perturbative calculations (59, 60, 61, 62, 63, 65, 64, 66, 67, 68, 69): Within Step 1 the matching of the effective couplings  $C_i$  at the high-energy scale  $\mu_0 \sim M_W$  requires a three-loop calculation for the cases  $i = 7, 8$  (59) and a two-loop calculation for the other cases (60). Within Step 2 the self-mixing of the four-quark operators ( $i = 1, \dots, 6$ ) and the self-mixing of the dipole operators ( $i = 7, 8$ ) have been calculated by a three-loop calculation of anomalous dimensions (61, 62), and the mixing of the four-quark operators into the dipole operators by a four-loop calculation (63). These two steps have established the effective couplings at the low scale  $\mu_b \sim m_b$  to NNLL precision. Thus, large logarithms of the form  $\alpha_s^{n+p}(m_b) \log^n(m_b/m_W)$ , ( $p = 0, 1, 2$ ), are resummed. Within Step 3, the calculation of the matrix elements

of the operators to NNLL precision, only the dominating contributions have been calculated or estimated by now. The dominating two-loop matrix element of the photonic dipole operator  $\mathcal{O}_7$  including the bremsstrahlung contributions has been calculated in Refs. (65, 64, 66, 67). The other important piece is the three-loop matrix elements of the four-quark operators, which has first been calculated within the so-called large- $\beta_0$  approximation (68). A calculation that goes beyond this approximation by employing an interpolation in the charm quark mass  $m_c$  from  $m_c > m_b$  to the physical  $m_c$  value has been presented in Ref. (69). In this interpolation the  $\alpha_s^2\beta_0$  result (68) is assumed to be a good approximation for the complete  $\alpha_s^2$  result for vanishing charm mass. It is this part of the NNLL calculation which is still open for improvement. Indeed a complete calculation of the three-loop matrix elements of the four-quark operators  $\mathcal{O}_{1,2}$  for vanishing charm mass is work in progress (70) and will cross-check this assumption and the corresponding error estimate due to the interpolation.

Some perturbative NNLL corrections have not yet been included in the present NNLL estimate, but they are expected to be smaller than the current perturbative uncertainty of 3%: the virtual and bremsstrahlung contributions to the  $(\mathcal{O}_7, \mathcal{O}_8)$  and  $(\mathcal{O}_8, \mathcal{O}_8)$  interferences at order  $\alpha_s^2$ , the NNLL bremsstrahlung contributions in the large- $\beta_0$ -approximation beyond the  $(\mathcal{O}_7, \mathcal{O}_7)$  interference term (which are already available (71)), the four-loop mixing of the four-quark operators into the operator  $\mathcal{O}_8$  (63), and the exact mass dependence of various matrix elements beyond the large  $\beta_0$  approximation (72, 70, 73).

In the present NNLL prediction (58), the reduction of the renormalization-scale dependence at the NNLL is shown in Fig. 2. The most important effect occurs for the charm mass  $\overline{\text{MS}}$  renormalization scale  $\mu_c$ , which has been the main source of uncertainty at the NLL. The current uncertainty of  $\pm 3\%$  due to higher-order  $[\mathcal{O}(\alpha_s^3)]$  effects can be estimated via the NNLL curves in Fig. 2. The reduction factor of the perturbative error is greater than a factor of three. The central value of the NNLL prediction is based on the choices  $\mu_b = 2.5$  GeV and  $\mu_c = 1.5$  GeV.

At NNLL QCD accuracy subdominant perturbative electroweak two-loop corrections are also relevant and have been calculated to be  $-3.6\%$  (74, 75, 76, 77). They are included in the present NNLL prediction.

**$B \rightarrow X_s \ell^+ \ell^-$**  Compared with the  $B \rightarrow X_s \gamma$  decay, the inclusive  $B \rightarrow X_s \ell^+ \ell^-$  decay presents a complementary and more complex test of the SM, given that different perturbative electroweak contributions add to the decay rate. This inclusive mode is also dominated by perturbative contributions, if one eliminates  $c\bar{c}$  resonances with the help of kinematic cuts. In the so-called perturbative  $q^2$ -windows below and above the resonances, namely in the low-dilepton-mass region  $1 \text{ GeV}^2 < q^2 = m_{\ell\ell}^2 < 6 \text{ GeV}^2$  as well as in the high-dilepton-mass region where  $q^2 > 14.4 \text{ GeV}^2$ , theoretical predictions for the invariant mass spectrum are dominated by the perturbative contributions. A theoretical precision of order 10% is possible.

Compared with the decay  $B \rightarrow X_s \gamma$ , the effective Hamiltonian (Eq. 5) contains two additional operators of  $\mathcal{O}(\alpha_{\text{em}})$ , the semileptonic operators  $\mathcal{O}_9$  and  $\mathcal{O}_{10}$ . Moreover, the first large logarithm of the form  $\log(m_b/m_W)$  already arises without gluons, because the operator  $\mathcal{O}_2$  mixes into  $\mathcal{O}_9$  at one loop. It is then convenient to redefine the dipole and semileptonic operators via  $\tilde{\mathcal{O}}_i = 16\pi^2/g_s^2\mathcal{O}_i$ ,

$\tilde{C}_i = g_s^2/(4\pi)^2 C_i$  for  $i = 7, \dots, 10$ . With this redefinition, one can follow the three calculational steps discussed above. In particular, after the reshufflings the one-loop mixing of the operator  $\mathcal{O}_2$  with  $\tilde{\mathcal{O}}_9$  appears formally at order  $\alpha_s$ . To LL precision, there is only  $\tilde{\mathcal{O}}_9$  with a non-vanishing tree-level matrix element and a non-vanishing coefficient.

It is well-known that this naïve  $\alpha_s$  expansion is problematic, since the formally-leading  $O(1/\alpha_s)$  term in  $C_9$  is accidentally small and much closer in size to an  $O(1)$  term. Thus, also specific higher order terms in the general expansion are numerically important.<sup>3</sup>

The complete NLL contributions have been presented (44, 78). For the NNLL calculation, many components were taken over from the NLL calculation of the  $B \rightarrow X_s \gamma$  mode. The additional components for the NNLL QCD precision have been calculated (60, 48, 61, 79, 80, 85, 83, 84, 82, 81, 86, 88, 87): Some new pieces for the matching to NNLL precision (Step 1) have been calculated in Ref. (60). To NNLL precision the large matching scale uncertainty of 16% at the NLL level is eliminated. In Step 2, the mixing of the four-quark operators into the semileptonic operator  $\mathcal{O}_9$  has been calculated (48, 61). In Step 3, the four-quark matrix elements including the corresponding bremsstrahlung contributions have been calculated for the low- $q^2$  region in Refs. (79, 80, 81), bremsstrahlung contribution for the forward-backward asymmetry in  $B \rightarrow X_s \ell^+ \ell^-$  in Refs. (85, 83, 84), and the four-quark matrix elements in the high- $q^2$  region in Refs. (82, 81, 86). The two-loop matrix element of the operator  $\mathcal{O}_9$  has been estimated using the corresponding result in the decay mode  $B \rightarrow X_u \ell \nu$  and also Padé approximation methods (88); this estimate has been further improved in Ref. (87).

More recently electromagnetic corrections were calculated: NLL quantum electrodynamics (QED) two-loop corrections to the Wilson coefficients are of  $O(2\%)$  (88). Also, in the QED one-loop corrections to matrix elements, large collinear logarithms of the form  $\log(m_b^2/m_\ell^2)$  survive integration if only a restricted part of the dilepton mass spectrum is considered. These collinear logarithms add another contribution of order  $+2\%$  in the low- $q^2$  region for  $B \rightarrow X_s \mu^+ \mu^-$  (89). For the high- $q^2$  region, one finds  $-8\%$  (90).

**$B \rightarrow X_d \gamma$  and  $B \rightarrow X_d \ell^+ \ell^-$**  The perturbative QCD corrections in the inclusive decays  $B \rightarrow X_d \gamma$  (91, 55, 56) and  $B \rightarrow X_d \ell^+ \ell^-$  (92, 93) can be treated completely analogously to those in the corresponding  $b \rightarrow s$  modes. The effective Hamiltonian is the same in these processes, up to the obvious replacement of the  $s$  quark field by the  $d$  quark field. However, because  $\lambda_u = V_{ub} V_{ud}^*$  for  $b \rightarrow d \gamma$  is not small with respect to  $\lambda_t = V_{tb} V_{td}^*$  and  $\lambda_c = V_{cb} V_{cd}^*$ , one must also account for the operators proportional to  $\lambda_u$ , namely  $\mathcal{O}_{1,2}^u$  in Eq. 5. The matching conditions  $C_i(m_W)$  and the solutions of the RGEs, which yield  $C_i(\mu_b)$ , coincide with those needed for the corresponding  $b \rightarrow s$  processes (91, 92).

<sup>3</sup>The  $B \rightarrow X_s \ell^+ \ell^-$  decay amplitude has the following structure ( $\kappa = \alpha_{\text{em}}/\alpha_s$ ):

$$\mathcal{A} = \kappa \left[ \mathcal{A}_{LL} + \alpha_s \mathcal{A}_{NLL} + \alpha_s^2 \mathcal{A}_{NNLL} + \mathcal{O}(\alpha_s^3) \right] \quad \text{with} \quad \mathcal{A}_{LL} \sim \alpha_s \mathcal{A}_{NLL} \quad (7)$$

A strict NNLL calculation of the squared amplitude  $\mathcal{A}^2$  should only include terms up to order  $\kappa^2 \alpha_s^2$ . However, in the numerical calculation, one also includes the term  $\mathcal{A}_{NLL} \mathcal{A}_{NNLL}$  of order  $\kappa^2 \alpha_s^3$  which are numerically important. These terms beyond the formal NNLL level are proportional to  $|C_7|^2$  and  $|C_8|^2$  and are scheme-independent. One can even argue that one picks up the dominant NNNLL QCD corrections because the missing NNNLL piece in the squared amplitude, namely  $\mathcal{A}_{LL} \mathcal{A}_{NNNNLL}$ , can safely be neglected (87).



### 2.3 Hadronic Power Corrections to Inclusive Modes

The inclusive modes  $B \rightarrow X_s \gamma$  and  $B \rightarrow X_s \ell^+ \ell^-$  are dominated by the partonic contributions. Indeed, if only the leading operator in the effective Hamiltonian ( $\mathcal{O}_7$  for  $B \rightarrow X_s \gamma$ ,  $\mathcal{O}_9$  for  $B \rightarrow X_s \ell^+ \ell^-$ ) is considered, the HME makes it possible to calculate the inclusive decay rates of a hadron containing a heavy quark, especially a  $b$  quark (24, 25, 26, 27, 28, 29). The optical theorem relates the inclusive decay rate of a hadron  $H_b$  to the imaginary part of the forward scattering amplitude

$$\Gamma(H_b \rightarrow X) = \frac{1}{2m_{H_b}} \Im \langle H_b | \mathbf{T} | H_b \rangle, \quad (8)$$

where the transition operator  $\mathbf{T}$  is given by  $\mathbf{T} = i \int d^4x T[\mathcal{H}_{\text{eff}}(x)\mathcal{H}_{\text{eff}}(0)]$ . The insertion of a complete set of states,  $|X\rangle\langle X|$ , leads to the standard formula for the decay rate:

$$\Gamma(H_b \rightarrow X) = \frac{1}{2m_{H_b}} \sum_X (2\pi)^4 \delta^4(p_i - p_f) |\langle X | \mathcal{H}_{\text{eff}} | H_b \rangle|^2. \quad (9)$$

It is then possible to construct an OPE of the operator  $\mathbf{T}$ , which is expressed as a series of local operators that are suppressed by powers of the  $b$  quark mass and written in terms of the  $b$  quark field:

$$T[\mathcal{H}_{\text{eff}}\mathcal{H}_{\text{eff}}] \stackrel{OPE}{=} \frac{1}{m_b} (\mathcal{O}_0 + \frac{1}{m_b} \mathcal{O}_1 + \frac{1}{m_b^2} \mathcal{O}_2 + \dots). \quad (10)$$

This construction is based on the parton-hadron duality. The sum is performed over all exclusive final states and that the energy release in the decay is large with respect to the QCD scale,  $\Lambda \ll m_b$ . With the help of the heavy quark effective theory (HQET) (94,95), namely the new heavy quark spin-flavor symmetries that arise in the heavy quark limit  $m_b \rightarrow \infty$ , the hadronic matrix elements within the OPE,  $\langle H_b | \mathcal{O}_i | H_b \rangle$ , can be further simplified. In this well-defined expansion, the free quark model is the first term in the constructed expansion in powers of  $1/m_b$  and, therefore, is the dominant contribution. In the applications to inclusive rare  $B$  decays, one finds no correction of order  $\Lambda/m_b$  to the free quark model approximation. The corrections to the partonic decay rate begin with  $1/m_b^2$  only, which implies the rather small numerical impact of the nonperturbative corrections on the decay rate of inclusive modes. However, there are more subtleties to consider if other than the leading operators are taken into account (see below).

**$B \rightarrow X_s \gamma$**  These techniques can be used directly in the decay  $B \rightarrow X_s \gamma$  to single out nonperturbative corrections to the branching fraction: If one neglects perturbative QCD corrections and assumes that the decay  $B \rightarrow X_s \gamma$  is due to the leading electromagnetic dipole operator  $\mathcal{O}_7$  alone, then the photon would always be emitted directly from the hard process of the  $b$  quark decay. One has to consider the time-ordered product  $T\mathcal{O}_7^+(x)\mathcal{O}_7(0)$ . Using the OPE for  $T\mathcal{O}_7^+(x)\mathcal{O}_7(0)$  and HQET methods, as discussed above, the decay width  $\Gamma(B \rightarrow X_s \gamma)$  reads (30,31) (modulo higher terms in the  $1/m_b$  expansion):

$$\Gamma_{B \rightarrow X_s \gamma}^{(\mathcal{O}_7, \mathcal{O}_7)} = \frac{\alpha_{\text{em}} G_F^2 m_b^5}{32\pi^4} |V_{tb} V_{ts}|^2 C_7^2(m_b) \left( 1 + \frac{\delta_{\text{rad}}^{\text{NP}}}{m_b^2} \right), \quad \delta_{\text{rad}}^{\text{NP}} = \frac{1}{2} \lambda_1 - \frac{9}{2} \lambda_2, \quad (11)$$

where  $\lambda_1$  and  $\lambda_2$  are the HQET parameters for the kinetic energy and the chromomagnetic energy, respectively. If the  $B \rightarrow X_s \gamma$  decay width is normalized by the (charmless) semileptonic one, the nonperturbative corrections of order  $1/m_b^2$  cancel out within the ratio  $\mathcal{B}(B \rightarrow X_s \gamma)/\mathcal{B}(B \rightarrow X_u \ell \nu)$ .

However, as noted in Ref. (96), there is no OPE for the inclusive decay  $B \rightarrow X_s \gamma$  if one considers operators beyond the leading electromagnetic dipole operator  $\mathcal{O}_7$ . Voloshin (97) has identified a contribution to the total decay rate in the interference of the  $b \rightarrow s \gamma$  amplitude due to the electromagnetic dipole operator  $\mathcal{O}_7$  and the charming penguin amplitude due to the current-current operator  $\mathcal{O}_2$ . This resolved photon contribution contains subprocesses in which the photon couples to light partons instead of connecting directly to the effective weak-interaction vertex (98). If one treats the charm quark as heavy, then it is possible to expand the contribution in local operators. The first term in this expansion may be the dominating one (96,99,100). This nonperturbative correction is suppressed by  $\lambda_2/m_c^2$  and is estimated to be of order 3% compared with the leading-order (perturbative) contribution to the decay rate  $\Gamma_{b \rightarrow s \gamma}$  which arises from the electromagnetic operator  $\mathcal{O}_7$ :

$$\frac{\Delta\Gamma_{B \rightarrow X_s \gamma}^{(\mathcal{O}_2, \mathcal{O}_7)}}{\Gamma_{b \rightarrow s \gamma}^{\text{LL}}} = -\frac{1}{9} \frac{C_2}{C_7} \frac{\lambda_2}{m_c^2} \simeq +0.03. \quad (12)$$

However, if the charm mass is assumed to scale as  $m_c^2 \sim \Lambda m_b$ , then the charm penguin contribution must be described by the matrix element of a nonlocal operator (96,99,100,101).

Recently, another example of such nonlocal matrix elements within the power-suppressed contributions to the decay  $B \rightarrow X_s \gamma$  was identified (101)—specifically, in the interference of the  $b \rightarrow s \gamma$  transition amplitude mediated by the electromagnetic dipole operator  $\mathcal{O}_7$ , where the  $b \rightarrow sg$  amplitude is mediated by the chromo-magnetic dipole operator  $\mathcal{O}_8$ , followed by the fragmentation of the gluon into an energetic photon and a soft quark-antiquark pair. A naïve dimensional estimate of these power corrections leads to

$$\frac{\Delta\Gamma_{B \rightarrow X_s \gamma}^{(\mathcal{O}_7, \mathcal{O}_8)}}{\Gamma_{b \rightarrow s \gamma}^{\text{LL}}} \sim \pi \alpha_s \frac{C_8}{C_7} \frac{\Lambda}{m_b}, \quad (13)$$

whereas an estimate using the vacuum insertion method for the nonlocal matrix elements indicates an effect of  $-3\%$ .

Power corrections to the high-energy part of the  $B \rightarrow X_s \gamma$  photon spectrum can be parameterized systematically in terms of subleading shape functions. For the interference of the  $\mathcal{O}_7$ – $\mathcal{O}_7$  pair, these nonlocal operators reduce to local operators, if one considers the total decay rate (102,103,104), whereas other resolved photon contributions to the total decay rate—such as the previously analyzed  $\mathcal{O}_7$ – $\mathcal{O}_8$  interference term (101)—cannot be described by a local OPE. A recent systematic analysis (98) of all resolved photon contributions related to other operators in the weak Hamiltonian establishes this breakdown of the local OPE within the hadronic power corrections as a generic result. Clearly, estimating such nonlocal matrix elements is very difficult, and an irreducible theoretical uncertainty of  $\pm(4-5)\%$  for the total  $CP$  averaged decay rate, defined with a photon-energy cut of  $E_\gamma = 1.6$  GeV, remains (98). This result strongly indicates that the theoretical efforts for the  $B \rightarrow X_s \gamma$  mode have reached the nonperturbative

boundaries. The complete effect of power corrections on  $CP$  asymmetries has not yet been estimated.

$B \rightarrow X_s \ell^+ \ell^-$  Hadronic power corrections in the decay  $B \rightarrow X_s \ell^+ \ell^-$  that scale with  $1/m_b^2$ ,  $1/m_b^3$  (30, 31, 105, 106, 107, 108), and  $1/m_c^2$  (100) have also been considered. They can be calculated quite analogously to those in the decay  $B \rightarrow X_s \gamma$ . However, a systematic analysis of hadronic power corrections including all relevant operators has yet to be performed. Thus, an additional uncertainty of  $\pm 5\%$  should be added to all theoretical predictions for this mode on the basis of a simple dimensional estimate.

In the high- $q^2$  region, one encounters the breakdown of the HME at the end point of the dilepton mass spectrum: Whereas the partonic contribution vanishes, the  $1/m_b^2$  and  $1/m_b^3$  corrections tend towards a nonzero value. In contrast to the end-point region of the photon-energy spectrum in the  $B \rightarrow X_s \gamma$  decay, no partial all-order resummation into a shape function is possible. However, for an integrated high- $q^2$  spectrum an effective expansion is found in inverse powers of  $m_b^{\text{eff}} = m_b \times (1 - \sqrt{s_{\text{min}}})$  rather than  $m_b$  (109, 110). The expansion converges less rapidly, depending on the lower dilepton-mass cut  $s_{\text{min}} = q_{\text{min}}^2/m_b^2$  (81).

The large theoretical uncertainties could be significantly reduced by normalizing the  $B \rightarrow X_s \ell^+ \ell^-$  decay rate to the semileptonic  $B \rightarrow X_u \ell \bar{\nu}$  decay rate with the same  $q^2$  cut (108):

$$\mathcal{R}(s_0) = \int_{\hat{s}_0}^1 d\hat{s} \frac{d\Gamma(B \rightarrow X_s \ell^+ \ell^-)}{d\hat{s}} / \int_{\hat{s}_0}^1 d\hat{s} \frac{d\Gamma(B^0 \rightarrow X_u \ell \nu)}{d\hat{s}}. \quad (14)$$

For example, the uncertainty due to the dominating  $1/m_b^3$  term would be reduced from 19% to 9% (89).

$B \rightarrow X_d \gamma$  The nonperturbative contributions in the decay  $B \rightarrow X_d \gamma$  can be treated analogously to those in the decay  $B \rightarrow X_s \gamma$ . The power corrections that scale as  $1/m_b^2$  (in addition to the CKM factors) are the same for the two modes. Also, the systematic analysis of resolved contributions given in Ref. (98) can be applied to this case. However, the long-distance contributions from the intermediate  $u$  quark in the penguin loops are critical. They are suppressed in the  $B \rightarrow X_s \gamma$  mode by the CKM matrix elements. In  $B \rightarrow X_d \gamma$ , there is no CKM suppression, and one must account for the nonperturbative contributions that arise from the operator  $\mathcal{O}_1^u$ . The contribution due to the  $\mathcal{O}_1^u$ - $\mathcal{O}_7$  interference scales with  $\Lambda/m_b$  (106). However, this interference contribution vanishes in the total  $CP$ -averaged rate of  $B \rightarrow X_s \gamma$  at order  $\Lambda/m_b$  (98). This result applies to the total rate of  $B \rightarrow X_d \gamma$  as well. Other interference terms, namely the double resolved contributions  $\mathcal{O}_1^u$ - $\mathcal{O}_8$  and  $\mathcal{O}_1^u$ - $\mathcal{O}_1^u$ , arise first at order  $1/m_b^2$ , as they can also be deduced from the results presented in Ref. (98). Thus, there is no power correction due to the operator  $\mathcal{O}_1^u$  in the total rate of  $B \rightarrow X_d \gamma$  at order  $\Lambda/m_b$ , which implies that the  $CP$ -averaged decay rate of  $B \rightarrow X_d \gamma$  is as theoretically clean as the decay rate of  $B \rightarrow X_s \gamma$ .

$B \rightarrow X_d \ell^+ \ell^-$  In the case of  $B \rightarrow X_d \ell^+ \ell^-$  long-distance contributions due to  $u$  quark loops can be avoided in the low- $q^2$  window  $1 \text{ GeV}^2 < q^2 < 6 \text{ GeV}^2$ . The  $\rho$  and  $\omega$  resonances are below, and the  $c\bar{c}$  ( $J/\psi$ ,  $\psi'$ ) resonances are above this window (92). The effect of their respective tails can be taken into account

within the Krüger-Sehgal (KS) approach (see Section 2.5) (111,112). In this low- $q^2$  region, one can then treat the nonperturbative power corrections analogously to those in the decay  $B \rightarrow X_s \ell^+ \ell^-$ , and one can expect a similar theoretical accuracy in this  $q^2$  window.

## 2.4 Nonperturbative Corrections due to Kinematical Cuts

There are additional subtleties in inclusive modes. Kinematical cuts induce additional sensitivities to nonperturbative physics.

**$B \rightarrow X_s \gamma$**  In the measurement of the inclusive mode  $B \rightarrow X_s \gamma$  one needs cuts in the photon-energy spectrum to suppress the background from other  $B$  decays (Fig. 3).

These shape-function effects were taken into account in the experimental analysis, and the corresponding theoretical uncertainties due to this model dependence are reflected in the extrapolation error of the experimental results (see Section 5.1). The extrapolation is done from the experimental energy cut values down to 1.6 GeV by use of three different theoretical schemes (114, 75, 115, 116) for averaging.

Again constraining the analysis to the leading operator  $\mathcal{O}_7$ , a cut around 1.6 GeV might not guarantee that a theoretical description in terms of a local OPE is sufficient because of the sensitivity to the scale  $\Delta = m_b - 2E_\gamma$  (117). A multiscale OPE with three short-distance scales  $m_b$ ,  $\sqrt{m_b \Delta}$ , and  $\Delta$  has been proposed to connect the shape function and the local OPE region. Recently, such additional perturbative cutoff-related effects have been calculated to NNLL precision by the use of SCET methods (118, 119, 120). Such perturbative effects due to the additional scale are negligible for 1.0 GeV but of order 3% at 1.6 GeV (118). The size of these effects at 1.6 GeV is similar to the 3% higher-order uncertainty in the present NNLL prediction. However, the numerical consistency of the SCET analysis has recently been questioned (121). Far away from the endpoint ( $E_0 = 1.6$  GeV), the logarithmic and nonlogarithmic terms cancel; the same result was presented in Ref. (122). Within the resummation of the cutoff-enhanced logarithms this feature leads to an overestimate of the  $O(\alpha_s^3)$  terms (121). Further work is needed to clarify this issue.

There is an alternative approach to the cut effects in the photon-energy spectrum that is based on dressed gluon exponentiation and on the incorporation of Sudakov and renormalon resummations (123, 122). The greater predictive power of this approach is related in part to the assumption that nonperturbative power corrections associated with the shape function follow the pattern of ambiguities present in the perturbative calculation (124). In the future, these additional perturbative cut effects could be analyzed and combined together with those already included in the experimental average.

**$B \rightarrow X_s \ell^+ \ell^-$**  In the inclusive decay  $B \rightarrow X_s \ell^+ \ell^-$ , the hadronic and dilepton invariant masses are independent kinematical quantities. A hadronic invariant-mass cut is imposed in the experiments (see Section 5.7). The high-dilepton-mass region is not affected by this cut, but in the low-dilepton mass region the kinematics with a jet-like  $X_s$  and  $m_X^2 \leq m_b \Lambda$  implies the relevance of the shape function. A recent SCET analysis shows that by using the universality of the shape function, a 10 – 30% reduction in the dilepton-mass spectrum can be

accurately computed. Nevertheless, the effects of subleading shape functions lead to an additional uncertainty of 5% (125,126). A more recent analysis (127) estimates the uncertainties due to subleading shape functions more conservatively. By scanning over a range of models of these functions, one finds corrections in the rates relative to the leading-order result to be between  $-10\%$  to  $+10\%$  with equally large uncertainties. In the future it may be possible to decrease such uncertainties significantly by constraining both the leading and subleading shape functions using the combined  $B \rightarrow X_s \gamma$ ,  $B \rightarrow X_u \ell \bar{\nu}$  and  $B \rightarrow X_s \ell^+ \ell^-$  data (127).

## 2.5 Charmonium Resonance Contributions

One must also consider the on-shell  $c\bar{c}$  resonances, which have to be taken out. Whereas in the decay  $B \rightarrow X_s \gamma$  the intermediate  $\psi$  background, namely  $B \rightarrow \psi X_s$  followed by  $\psi \rightarrow X' \gamma$ , is suppressed for the high-energy cut  $E_\gamma$  and can be subtracted from the  $B \rightarrow X_s \gamma$  decay rate, the  $c\bar{c}$  resonances show up as large peaks in the dilepton-invariant mass spectrum in the decay  $B \rightarrow X_s \ell^+ \ell^-$ .

As discussed in Section 2.2, these resonances can be removed by making appropriate kinematic cuts in the invariant mass spectrum. However, nonperturbative contributions away from the resonances within the perturbative windows are also important. In the KS approach (111,112) one absorbs factorizable long-distance charm rescattering effects (in which the  $B \rightarrow X_s c\bar{c}$  transition can be factorized into the product of  $\bar{s}b$  and  $c\bar{c}$  color-singlet currents) into the matrix element of the leading semileptonic operator  $\mathcal{O}_9$ . Following the inclusion of nonperturbative corrections scaling with  $1/m_c^2$ , the KS approach avoids double-counting. For the integrated branching fractions one finds an increase of  $(1-2)\%$  in the low- $q^2$  region due to the KS effect, whereas in the high- $q^2$  region the increase is well below the uncertainty due to the  $1/m_b$  corrections. As shown in Fig. 3, the integrated branching fraction is dominated by this resonance background which exceeds the nonresonant charm-loop contribution by two orders of magnitude. This feature should not be misinterpreted as a striking failure of global parton-hadron duality (113), which postulates that the sum over the hadronic final states, including resonances, should be well approximated by a quark-level calculation (128). Crucially, the charm-resonance contributions to the decay  $B \rightarrow X_s \ell^+ \ell^-$  are expressed in terms of a phase-space integral over the absolute square of a correlator. For such a quantity global quark-hadron duality is not expected to hold. Nevertheless, local quark-hadron duality (which, of course, also implies global duality) may be reestablished by resumming Coulomb-like interactions (113).

## 2.6 Soft Collinear Effective Theory for Exclusive Decays

The Wilson coefficients of the weak effective Hamiltonian are process-independent and therefore can be used directly in the description of exclusive modes. It is computing of the hadronic matrix elements between meson states that is difficult in the case of exclusive modes and that limits the theoretical precision. The naïve approach consists of writing the amplitude  $A \simeq C_i(\mu_b) \langle \mathcal{O}_i(\mu_b) \rangle$  and parameterizing  $\langle \mathcal{O}_i(\mu_b) \rangle$  in terms of form factors. A substantial improvement can be obtained by using the QCDF method (32, 33, 34) and its field-theoretical formulation, the SCET method (35, 36, 37, 38, 39, 40). These methods form the basis of the up-to-date predictions of exclusive  $B$  decays. Within this framework one can show that, even if the form factors were known with infinite precision, the

description of exclusive decays would be incomplete due to the existence of so-called nonfactorizable strong interaction effects that do not correspond to form factors.

The QCDF and SCET methods were first systematized for nonleptonic decays in the heavy quark limit. In contrast to the HQET, SCET does not correspond to a local operator expansion. Whereas HQET is applicable to  $B$  decays if the energy transfer to light hadrons is small, for example to  $B \rightarrow D$  transitions at small recoil to the  $D$  meson, HQET is not applicable if some of the outgoing, light particles have momenta of order  $m_b$ . If so, one faces a multi-scale problem that can be tackled within SCET. In this case, there are three relevant scales: (a)  $\Lambda = \text{few} \times \Lambda_{\text{QCD}}$ , the soft scale set by the typical energies and momenta of the light degrees of freedom in the hadronic bound states; (b)  $m_b$ , the hard scale set by both the heavy  $b$  quark mass and the energy of the final-state hadron in the  $B$  meson rest frame; and (c) the hard-collinear scale  $\mu_{\text{hc}} = \sqrt{m_b \Lambda}$ , which appears through interactions between the soft and energetic modes in the initial and final states. The dynamics of hard and hard-collinear modes can be described perturbatively in the heavy quark limit  $m_b \rightarrow \infty$ . Thus, SCET describes  $B$  decays to light hadrons with energies much larger than their masses, assuming that their constituents have momenta collinear to the hadron momentum.

**$B \rightarrow K^* \gamma$  and  $B \rightarrow \rho \gamma$**  The application of the QCDF formalism to radiative and semileptonic decays was first proposed in Ref. (129). For  $B \rightarrow K^* \gamma$ , or more generally for  $B \rightarrow V \gamma$ , where  $V$  is a light vector meson, the QCDF formula for the hadronic matrix element of each operator of the effective Hamiltonian in the heavy quark limit and to all orders in  $\alpha_s$  reads

$$\langle V \gamma | \mathcal{O}_i | B \rangle = T_i^I F^{B \rightarrow V_\perp} + \int_0^\infty \frac{d\omega}{\omega} \phi_B(\omega) \int_0^1 du \phi_{V_\perp}(u) T_i^{II}(\omega, u). \quad (15)$$

This formula separates the process-independent nonperturbative quantities  $F^{B \rightarrow V_\perp}$ , a form factor evaluated at maximum recoil ( $q^2 = 0$ ), and  $\phi_B$  and  $\phi_{V_\perp}$ , the light-cone distribution amplitudes (LCDAs) for the heavy and light mesons, respectively, from the perturbatively calculable quantities  $T^I$  and  $T^{II}$ . The latter correspond to vertex and spectator corrections, respectively, and have been calculated to  $O(\alpha_s^1)$  (130, 131, 132, 133). More recently, some  $\alpha_s^2$  terms were also presented (134).

Light-cone wave functions of pseudo-scalar and vector mesons that enter the factorization formula have been studied in detail through the use of light-cone QCD sum rules (135, 136, 137, 138). However, not much is known about the  $B$  meson LCDA, whose first negative moment enters the factorized amplitude at  $O(\alpha_s)$ . Because this moment also enters the factorized expression for the  $B \rightarrow \gamma$  form factor, it might be possible to extract its value from measurements of decays such as  $B \rightarrow \gamma e \nu$ , if the power corrections are under control.

The QCDF formula also includes an important simplification in the form factor description. The  $B \rightarrow V$  form factors at large recoil have been analyzed in SCET (139, 140, 141) and are independent of the Dirac structure of the current in the heavy quark limit; as a consequence, all  $B \rightarrow V_\perp$  form factors reduce to a single form factor up to factorizable corrections in the heavy quark and large energy limits (142, 129).

Field-theoretical methods such as SCET make it possible to reach a deeper understanding of the QCDF approach. The various momentum regions are repre-

sented by different fields in the effective field theory. The hard-scattering kernels  $T^I$  and  $T^{II}$  can be shown to be Wilson coefficients of effective field operators. Using SCET one can prove the factorization formula to all orders in  $\alpha_s$  and to leading order in  $\Lambda/m_b$  (143). QCD is matched on SCET in a two-step procedure that separates the hard scale  $\mu \sim m_b$  and then the hard-collinear scale  $\mu \sim \sqrt{\Lambda m_b}$  from the hadronic scale  $\Lambda$ . The vertex correction term  $T^I$  involves the hard scales, whereas the spectator scattering term  $T^{II}$  involves both the hard and the hard-collinear scales. This is why large logarithms have to be resummed (143), which can be done most efficiently in SCET.

In principle, the field-theoretical framework of SCET allows one to go beyond the leading-order result in  $\Lambda/m_b$  (144). However, a breakdown of factorization is expected at that order (34). For example, in the analysis of  $B \rightarrow K^* \gamma$  decays at subleading order, an infrared divergence is encountered in the matrix element of  $\mathcal{O}_8$  (145). In general, power corrections involve convolutions, which turn out to be divergent. Currently, no solution to this well-analyzed problem of end-point divergences within power corrections is available (146, 140, 147). Thus, within the QCDF/SCET approach, a general, quantitative method to estimate the important  $\Lambda/m_b$  corrections to the heavy quark limit is missing, which significantly limits the precision in phenomenological applications.

Nevertheless, some very specific power corrections are still computable and are often numerically important. Indeed, this is the case for the annihilation and weak exchange amplitudes in  $B \rightarrow \rho \gamma$ . The annihilation contributions also represent the leading contribution to isospin asymmetries (145). All these corrections are included in recent analyses of radiative exclusive decays (148, 149, 150). Moreover, the method of light-cone QCD sum rules can help provide estimates of such unknown subleading terms. For example, power corrections for the indirect  $CP$  asymmetries in  $B \rightarrow V \gamma$  decays have been analyzed in this manner (151).

**$B \rightarrow K^{(*)} \ell^+ \ell^-$**  There is also a factorization formula for the exclusive semileptonic  $B$  decays, such as  $B \rightarrow K^* \ell^+ \ell^-$ , that are analogous to the one for the radiative decay  $B \rightarrow K^* \gamma$  (130, 150). The simplification due to form factor relations is even more drastic. The hadronic form factors can be expanded in the small ratios  $\Lambda/m_b$  and  $\Lambda/E$ , where  $E$  is the energy of the light meson. If we neglect corrections of order  $1/m_b$  and  $\alpha_s$ , the seven a priori independent  $B \rightarrow K^*$  form factors reduce to two universal form factors  $\xi_\perp$  and  $\xi_\parallel$  (142, 129). This reduction makes it possible to design interesting ratios of observables in which any soft form factor dependence cancels out for all dilepton masses  $q^2$  at leading order in  $\alpha_s$  and  $\Lambda/m_b$  (152).

The theoretical simplifications of the QCDF/SCET approach are restricted to the kinematic region in which the energy of the  $K^*$  is of the order of the heavy quark mass; that is,  $q^2 \ll m_B^2$ . Moreover, the influences of very light resonances below  $1 \text{ GeV}^2$  question the QCDF results in this region. In addition, the longitudinal amplitude in the QCDF/SCET approach generates a logarithmic divergence in the limit  $q^2 \rightarrow 0$ , which indicates problems in the theoretical description below  $1 \text{ GeV}^2$  (130). Thus, the factorization formula applies well in the dilepton mass range  $1 \text{ GeV}^2 < q^2 < 6 \text{ GeV}^2$ .

Clearly, the QCDF and SCET methods are also applicable to the phenomenologically important semileptonic decays such as  $B \rightarrow K \ell^+ \ell^-$  (130, 153),  $B \rightarrow \rho \ell^+ \ell^-$  (150), and  $B_s \rightarrow \phi \ell^+ \ell^-$ . The decay mode into a pseudoscalar is analogous

to the decay mode into a longitudinal vector meson.

### 3 EXPERIMENTAL TECHNIQUES

The  $\Upsilon(4S)$  resonance produced by the  $e^+e^-$  collision at the  $B$  factories provides a clean sample of  $B^0\bar{B}^0$  and  $B^+B^-$  meson pairs as well as strong kinematical constraints that are otherwise unavailable, particularly at hadron colliders. The main background is from continuum light quark pair production ( $e^+e^- \rightarrow q\bar{q}$ ,  $q = u, d, s, c$ ), which has a cross section only three times larger than that of  $B\bar{B}$  production. Radiative and electroweak penguin  $B$  decays are efficiently measured at the  $B$  factories thanks to their clear signatures: a high-energy photon and a lepton pair, respectively.

#### 3.1 Exclusive $B$ Reconstruction

A  $B$  meson decaying into an exclusive final state is reconstructed by measuring all long-lived decay products ( $\pi^\pm$ ,  $K^\pm$ ,  $e^\pm$ ,  $\mu^\pm$  and  $\gamma$ ), selecting intermediate states of certain invariant masses, and calculating two standard variables: the beam-energy constrained mass  $M_{bc} = \sqrt{s/4 - |p_B^*|^2}$  (also referred to as the beam-energy substituted mass,  $M_{ES}$ ) and the energy difference  $\Delta E = E_B^* - \sqrt{s}/2$ . Here,  $\sqrt{s}/2$  is the beam energy, and  $p_B^*$  and  $E_B^*$  are the momentum and energy, respectively, of the reconstructed  $B$  meson candidate in the  $\Upsilon(4S)$  rest frame.

$M_{bc}$  has a peak at the  $B$  meson mass and  $\Delta E$  has a peak at zero (Fig. 4). The resolution of  $M_{bc}$  is significantly better than that of  $\Delta E$ , as the former is dominated by the spread of the beam energy, whereas the latter is dominated by the detector resolution. The  $\Delta E$  variable is sensitive to misreconstructed background events, whereas  $M_{bc}$  has little separation power for them. When a kaon is misidentified as a pion,  $\Delta E$  shifts by approximately 50 MeV, and when a low momentum pion is added or missed,  $\Delta E$  shifts by more than the pion mass. An exclusive  $b \rightarrow d\gamma$  final state is thus separated from a similar  $b \rightarrow s\gamma$  state with  $\Delta E$ , but this separation is marginal due to the photon energy resolution of the electromagnetic calorimeter. Therefore, pion to kaon separation is crucial for the measurement of the suppressed  $b \rightarrow d\gamma$  processes.

Background events due to random combinations of particles are also reduced by correctly identifying particle species. For the  $b \rightarrow s\ell^+\ell^-$  processes, electrons and muons are almost completely separated from the more abundant hadrons. In addition, various techniques based on the event topology can be applied to suppress the background from continuum  $q\bar{q}$  events.

#### 3.2 Inclusive Measurement Techniques

A fully inclusive measurement of  $B \rightarrow X_s\gamma$ , in which the system recoiling against the emitted photon is not reconstructed, has been performed at the  $B$  factories thanks to the clean environment. The dominant background photon sources are (a) the copiously produced  $\pi^0 \rightarrow \gamma\gamma$  decays, (b)  $\eta \rightarrow \gamma\gamma$  to a lesser extent, and (c) other secondary and initial-state radiation photons in continuum  $q\bar{q}$  events. These contributions can be safely subtracted because they are measured in events taken 60 or 40 MeV below the  $\Upsilon(4S)$  resonance (i.e., off resonance). Here, small corrections due to the center-of-mass energy difference are applied to the production cross section and the reconstruction efficiency. To avoid sacrificing the



$B$  decay sample for other studies, the size of the off-resonance data sample is only  $\sim 10\%$  of the on-resonance sample from both Belle and BaBar and is the dominant source of statistical and systematic errors (CLEO collected one-third of the sample as off-resonance). The second severe background source arises from similar secondary photons from  $B$  decays. These contributions are subtracted from the expected photon spectrum on the basis of measured  $\pi^0$  and  $\eta$  spectra from  $B$  decays, various control samples, or Monte Carlo simulation.

An alternative technique is to measure as many exclusive modes as possible and then calculate their sum (i.e., the sum-of-exclusive method). Exclusive branching fractions measured to date do not saturate the inclusive process, but one can still infer the total branching fraction by estimating the fraction of unmeasured modes of typically  $\sim 45\%$  (or  $\sim 30\%$  if  $K_L^0$  modes are accounted for by corresponding  $K_S^0$  modes) using simulated hadronization processes. In the simulation, a light quark pair is generated according to the SM mass spectrum and final-state hadrons are produced by the PYTHIA program (155). This method also provides direct information about the  $B$  meson. For example, the  $B$  meson momentum defines the  $B$  meson rest frame, and charge and flavor information allows  $CP$ - and isospin-asymmetry measurements. So far, the sum-of-exclusive method is the only way to perform inclusive measurements of  $B \rightarrow X_s \ell^+ \ell^-$  and  $B \rightarrow X_d \gamma$  decays.

Another potentially definitive method is the so-called  $B$ -reco technique, in which the other  $B$  meson is fully reconstructed, thereby allowing the target  $B$  decay to be measured in a very clean environment. The efficiency is as low as a fraction of a percent, and will be more important in future experiments.

## 4 PRESENT THEORETICAL PREDICTIONS

Theoretical predictions have significantly improved in the past decade along with the development of the theoretical tools. There have also been improvements in the relevant experimental input quantities, as discussed below.

### 4.1 Inclusive Penguin Decays

The inclusive radiative and electroweak penguin modes offer theoretically clean observables because nonperturbative corrections are small and well under control. This assessment also applies to the branching fraction of  $B \rightarrow X_d \gamma$  mode as discussed in Section 2.3.

**Inclusive  $B \rightarrow X_s \gamma$**  The stringent bounds obtained from  $B \rightarrow X_s \gamma$  on various nonstandard scenarios are a clear example of the importance of clean FCNC observables for discriminating NP models.

The branching fraction for  $B \rightarrow X_q \gamma$  ( $q = s, d$ ) can be parameterized as

$$\mathcal{B}(B \rightarrow X_q \gamma)_{E_\gamma > E_0} = \mathcal{B}(B \rightarrow X_c e \bar{\nu})_{\text{exp}} \frac{6\alpha_{\text{em}}}{\pi C} \left| \frac{V_{tq}^* V_{tb}}{V_{cb}} \right|^2 \left[ P(E_0) + N(E_0) \right], \quad (16)$$

where  $\alpha_{\text{em}} = \alpha_{\text{em}}^{\text{onshell}}$  (74),  $C = |V_{ub}|^2 / |V_{cb}|^2 \times \Gamma[B \rightarrow X_c e \bar{\nu}] / \Gamma[B \rightarrow X_u e \bar{\nu}]$  and  $P(E_0)$  and  $N(E_0)$  denote the perturbative and nonperturbative contributions, respectively. The latter are normalized to the charmless semileptonic rate to separate the charm dependence.

The first NNLL prediction, which is based on the perturbative calculations discussed in Section 2.2 and on the analyses of nonperturbative corrections presented in Sections 2.3 and 2.4, for a photon-energy cut  $E_\gamma > 1.6$  GeV (58), reads as:

$$\mathcal{B}(B \rightarrow X_s \gamma)_{\text{NNLL}} = (3.15 \pm 0.23) \times 10^{-4}. \quad (17)$$

The overall uncertainty consists of nonperturbative (5%), parametric (3%), perturbative (scale) (3%) and  $m_c$ -interpolation ambiguity (3%), which are added in quadrature. An additional scheme dependence in the determination of the prefactor  $C$  has been found (156); it is within the perturbative uncertainty of 3% (121).

Thus, the SM prediction and the experimental average (see Section 5.1) are consistent at the  $1.2\sigma$  level. This finding implies very stringent constraints on NP models, such as (a) the bound on the charged Higgs mass in the two-Higgs doublet model (157, 158) ( $M_{H^+} > 295$  GeV at 95% CL) (58) and (b) the bound on the inverse compactification radius of the minimal universal extra dimension model ( $1/R > 600$  GeV at 95% CL) (159). In both cases, the bounds are much stronger than those derived from other measurements. Constraints within various supersymmetric extensions have been analyzed in Refs. (160, 161, 162, 163, 164, 165, 166, 167, 168) (for overviews see (16, 169)). Bounds on the little Higgs model with  $T$ -parity have also been presented (170). Finally, model-independent analyses in the effective field theory approach without (171) and with the assumption of minimal flavor violation (172, 173) also show the strong constraining power of the  $B \rightarrow X_s \gamma$  branching fraction.

**Inclusive  $B \rightarrow X_d \gamma$**  The theoretical predictions for the branching fraction  $\mathcal{B}(B \rightarrow X_d \gamma)$  for photon energies  $E_\gamma > 1.6$  GeV read as (55, 56):

$$\mathcal{B}(B \rightarrow X_d \gamma) = \left( 1.38 \begin{smallmatrix} +0.14 \\ -0.21 \end{smallmatrix} \Big|_{\frac{m_c}{m_b}} \pm 0.15_{\text{CKM}} \pm 0.09_{\text{param.}} \pm 0.05_{\text{scale}} \right) \times 10^{-5}, \quad (18)$$

and

$$\frac{\mathcal{B}(B \rightarrow X_d \gamma)}{\mathcal{B}(B \rightarrow X_s \gamma)} = \left( 3.82 \begin{smallmatrix} +0.11 \\ -0.18 \end{smallmatrix} \Big|_{\frac{m_c}{m_b}} \pm 0.42_{\text{CKM}} \pm 0.08_{\text{param.}} \pm 0.15_{\text{scale}} \right) \times 10^{-2}. \quad (19)$$

These predictions are of NLL order. They are fully consistent with previous results (91). A good part of the uncertainties cancel out in the ratio. The errors are dominated by CKM uncertainties, and thus the measurement of  $\mathcal{B}(B \rightarrow X_d \gamma)$  constrains the CKM parameters. This measurement is also of specific interest with respect to NP, because its CKM suppression by the factor  $|V_{td}|^2/|V_{ts}|^2$  in the SM may not hold in extended models.

**Direct  $CP$  Asymmetry** Other important observables are the direct  $CP$  asymmetries ( $q = s, d$ ), whose sign is always defined in terms of  $b - \bar{b}$ , or

$$\mathcal{A}_{CP}(\bar{B} \rightarrow X_q \gamma) \equiv \frac{\Gamma(\bar{B} \rightarrow X_q \gamma) - \Gamma(B \rightarrow X_{\bar{q}} \gamma)}{\Gamma(\bar{B} \rightarrow X_q \gamma) + \Gamma(B \rightarrow X_{\bar{q}} \gamma)}. \quad (20)$$

As first noted in Ref. (174), the SM predictions are almost independent from the photon energy cut-off and, for  $E_\gamma > 1.6$  GeV, read as (55, 56)

$$\mathcal{A}_{CP}(\bar{B} \rightarrow X_s \gamma) = \left( 0.44 \begin{smallmatrix} +0.15 \\ -0.10 \end{smallmatrix} \Big|_{\frac{m_c}{m_b}} \pm 0.03_{\text{CKM}} \begin{smallmatrix} +0.19 \\ -0.09 \end{smallmatrix} \Big|_{\text{scale}} \right) \times 10^{-2}, \quad (21)$$

and

$$\mathcal{A}_{CP}(\overline{B} \rightarrow X_d \gamma) = \left( -10.2 \left. \begin{smallmatrix} +2.4 \\ -3.7 \end{smallmatrix} \right|_{\frac{m_c}{m_b}} \pm 1.0_{\text{CKM}} \left. \begin{smallmatrix} +2.1 \\ -4.4 \end{smallmatrix} \right|_{\text{scale}} \right) \times 10^{-2}. \quad (22)$$

The two  $CP$  asymmetries are connected by the relative CKM factor  $\lambda^2 [(1-\rho)^2 + \eta^2]$ . The small SM prediction for the  $CP$  asymmetry in the decay  $B \rightarrow X_s \gamma$  is a result of three suppression factors: (a)  $\alpha_s$  to have a strong phase; (b) CKM suppression of order  $\lambda^2$ ; and (c) GIM suppression of order  $(m_c/m_b)^2$ , which reflects that in the limit  $m_c = m_u$ , any  $CP$  asymmetry in the SM would vanish.

On the basis of CKM unitarity, one can derive the following  $U$ -spin relation between the un-normalized  $CP$  asymmetries (175):

$$\left[ \Gamma(\overline{B} \rightarrow X_s \gamma) - \Gamma(B \rightarrow X_{\overline{s}} \gamma) \right] + \left[ \Gamma(\overline{B} \rightarrow X_d \gamma) - \Gamma(B \rightarrow X_{\overline{d}} \gamma) \right] = 0 \quad (23)$$

$U$ -spin breaking effects can be estimated within the HME (even beyond the partonic level), so one arrives at the following prediction for the total (or untagged)  $\overline{B} \rightarrow X_{s+d} \gamma$  asymmetry (176, 177):

$$|\Delta \mathcal{B}(\overline{B} \rightarrow X_s \gamma) + \Delta \mathcal{B}(\overline{B} \rightarrow X_d \gamma)| \sim 1 \cdot 10^{-9}. \quad (24)$$

Because this null test is based on the CKM unitarity, it represents a clear test for new  $CP$  phases beyond the CKM phase (176, 177). NP sensitivities of direct  $CP$  asymmetries have been analyzed (174, 55).

**Inclusive  $B \rightarrow X_s \ell^+ \ell^-$**  The decay  $B \rightarrow X_s \ell^+ \ell^-$  is particularly attractive because it offers several kinematic observables. The angular decomposition of the decay rate provides three independent observables,  $H_T$ ,  $H_A$  and  $H_L$ , from which one can extract the short-distance electroweak Wilson coefficients that test for NP (178):

$$\frac{d^3 \Gamma}{dq^2 dz} = \frac{3}{8} [(1+z^2)H_T(q^2) + 2(1-z^2)H_L(q^2) + 2zH_A(q^2)]. \quad (25)$$

Here  $z = \cos \theta_\ell$ ,  $\theta_\ell$  is the angle between the negatively charged lepton and the  $\overline{B}$  meson in the center-of-mass frame of the dilepton system, and  $q^2$  is the dilepton mass squared.  $H_A$  is equivalent to the forward-backward asymmetry, and the dilepton-mass spectrum is given by  $H_T + H_L$ . The observables depend on the Wilson coefficients  $C_7$ ,  $C_9$  and  $C_{10}$  in the SM. The present measurements of the  $B \rightarrow X_s \ell^+ \ell^-$  already favor the SM-sign of the coefficient  $C_7$ , which is undetermined by the  $B \rightarrow X_s \gamma$  mode (179).

As discussed above, these observables are dominated by perturbative contributions in the perturbative low- and high- $q^2$  windows which are below ( $1 \text{ GeV}^2 < q^2 < 6 \text{ GeV}^2$ ), and above ( $q^2 > 14.4 \text{ GeV}^2$ ) the  $c\overline{c}$  resonances, respectively. The present predictions are based on the perturbative calculations to NNLL precision in QCD and to NLL precision in QED (see Section 2.2). For the branching fraction in the low- $q^2$  region one arrives at (89)

$$\mathcal{B}(B \rightarrow X_s \ell^+ \ell^-)_{\text{low}} = \begin{cases} (1.59 \pm 0.11) \times 10^{-6} & (\ell = \mu) \\ (1.64 \pm 0.11) \times 10^{-6} & (\ell = e), \end{cases} \quad (26)$$

and for the high- $q^2$  region, one arrives at (90)

$$\mathcal{B}(B \rightarrow X_s \ell^+ \ell^-)_{\text{high}} = \begin{cases} 2.40 \times 10^{-7} \times (1_{-0.26}^{+0.29}) & (\ell = \mu) \\ 2.09 \times 10^{-7} \times (1_{-0.30}^{+0.32}) & (\ell = e). \end{cases} \quad (27)$$

As suggested in Ref. (108), normalizing the  $B \rightarrow X_s \ell^+ \ell^-$  decay rate in the high- $q^2$  region to the semileptonic  $B \rightarrow X_u \ell \bar{\nu}$  decay rate with the same  $q^2$  cut (Eq. 14), significantly reduces the nonperturbative uncertainties (90):

$$\mathcal{R}(\hat{q}_0^2 = 14.4 \text{ GeV}^2) = \begin{cases} 2.29 \times 10^{-3} \times (1 \pm 0.13) & (\ell = \mu) \\ 1.94 \times 10^{-3} \times (1 \pm 0.16) & (\ell = e). \end{cases} \quad (28)$$

The value of  $q_0^2$  for which the forward-backward asymmetry vanishes,

$$(q_0^2)[X_s \ell^+ \ell^-] = \begin{cases} (3.50 \pm 0.12) \text{ GeV}^2 & (\ell = \mu) \\ (3.38 \pm 0.11) \text{ GeV}^2 & (\ell = e), \end{cases} \quad (29)$$

is one of the most precise predictions in flavor physics and also determines the relative sign and magnitude of the coefficients  $C_7$  and  $C_9$  (90). However, unknown subleading nonperturbative corrections of order  $O(\alpha_s \Lambda/m_b)$ , which are estimated to give an additional uncertainty of order 5%, have to be added in all observables of the  $B \rightarrow X_s \ell^+ \ell^-$  mode (see Section 2.3).

In all predictions, it is assumed that there is no cut in the hadronic mass region (see Section 2.4). Furthermore, after including the NLL QED matrix elements, the electron and muon channels receive different contributions due to terms involving  $\ln(m_b^2/m_\ell^2)$  (see Section 2.2). This is the only source of the difference between these two channels. All collinear photons are assumed to be included in the  $X_s$  system, and the dilepton invariant mass does not contain any photons; in other words,  $q^2 = (p_{\ell^+} + p_{\ell^-})^2$ . Present experimental settings at the  $B$  factories are different, and therefore the theoretical predictions have to be modified (87).

This difference in the settings also means that deviations from the SM prediction ( $R_{X_s}^{\text{SM}} = 1$ ) in the muon-electron ratio

$$R_{X_s} = \Gamma(B \rightarrow X_s \mu^+ \mu^-)_{[q_a^2, q_b^2]} / \Gamma(B \rightarrow X_s e^+ e^-)_{[q_a^2, q_b^2]} \quad (30)$$

can result from a different treatment of collinear photons in the two modes. This ratio is interesting because it is sensitive to the neutral Higgs boson of two-Higgs-doublet models at large  $\tan \beta$  (180,181), which is also valid in corresponding ratios  $R_{K^{(*)}}$  of exclusive modes: In the SM, one finds  $R_K = 1$ , as well as  $R_{K^*} = 0.75$  when integrated over all  $q^2$ , including  $M_{e^+e^-} < 2m_\mu$ .

## 4.2 Exclusive Penguin Decays

The exclusive penguin modes offer a larger variety of experimentally accessible observables than do the inclusive ones, but the nonperturbative uncertainties in the theoretical predictions are in general sizable.

**$B \rightarrow K^* \gamma$  and  $B \rightarrow \rho \gamma$**  The large hadronic uncertainties, which arise from the nonperturbative input of the QCDF formula and from our limited knowledge of power corrections, do not allow precise predictions of the branching fractions of exclusive modes. However, within ratios of exclusive modes such as asymmetries, parts of the uncertainties cancel out and one may hope for higher precision.

The ratio  $R_{\text{th}}(\rho\gamma/K^*\gamma)$  [and similarly  $R_{\text{th}}(\omega\gamma/K^*\gamma)$ ] is given by (148,149,150,151).

$$R_{\text{th}}(\rho\gamma/K^*\gamma) = \frac{\mathcal{B}_{\text{th}}(B \rightarrow \rho\gamma)}{\mathcal{B}_{\text{th}}(B \rightarrow K^*\gamma)} = S_\rho \left| \frac{V_{td}}{V_{ts}} \right|^2 \frac{(M_B^2 - m_\rho^2)^3}{(M_B^2 - m_{K^*}^2)^3} \zeta^2 [1 + \Delta R(\rho/K^*)], \quad (31)$$

where  $m_\rho$  is the mass of the  $\rho$  meson;  $\zeta$  is the ratio of the transition form factors,  $\zeta = \overline{T}_1^\rho(0)/\overline{T}_1^{K^*}(0)$ ; and  $S_\rho = 1$  and  $1/2$  for the  $\rho^\pm$  and  $\rho^0$  mesons, respectively. The quantity  $(1 + \Delta R)$  entails the explicit  $O(\alpha_s)$  corrections as well as the power-suppressed contributions. These functions also depend on CKM parameters, namely  $\phi_2 \equiv \alpha = \arg(-V_{cb}V_{cb}^*/V_{td}V_{tb}^*)$  and  $R_{ut} = |V_{ud}V_{ub}^*/V_{td}V_{tb}^*|$ , and one finds numerically (150) that

$$\Delta R(\rho^\pm/K^{*\pm}) = \left\{ 1 - 2R_{ut} \cos \phi_2 [0.24_{-0.18}^{+0.18}] + R_{ut}^2 [0.07_{-0.07}^{+0.12}] \right\}, \quad (32)$$

and

$$\Delta R(\rho^0/K^{*0}) = \left\{ 1 - 2R_{ut} \cos \phi_2 [-0.06_{-0.06}^{+0.06}] + R_{ut}^2 [0.02_{-0.01}^{+0.02}] \right\}. \quad (33)$$

These results are consistent with the predictions given in Refs. (148, 149, 151). Obviously, the neutral mode is better suited for the determination of  $|V_{td}/V_{ts}|$  than is the charged mode, in which the function  $\Delta R$  is dominated by the weak-annihilation contribution, which leads to a larger error. The most recent determination of the ratio  $\zeta = \overline{T}_1^\rho(0)/\overline{T}_1^{K^*}(0)$  within the light-cone QCD sum rule approach (182),  $1/\zeta = 1.17 \pm 0.09$ , leads to the determination of  $|V_{td}/V_{ts}|$  via Eq. (31) (see Section 5.4). However, the experimental data on the branching fractions of  $B \rightarrow K^*\gamma$  and  $B \rightarrow \rho\gamma$  calls for a larger error on  $\zeta$ , if one assumes no large power corrections beyond the known annihilation terms (150).

**Isospin Asymmetry in Radiative Decays** Another important observable is the isospin breaking ratio given by

$$\Delta_{0+}(B \rightarrow K^*\gamma) = \frac{\Gamma(B^0 \rightarrow K^{*0}\gamma) - \Gamma(B^+ \rightarrow K^{*+}\gamma)}{\Gamma(B^0 \rightarrow K^{*0}\gamma) + \Gamma(B^+ \rightarrow K^{*+}\gamma)}, \quad (34)$$

where the partial decay rates are  $CP$ -averaged. In the SM spectator-dependent effects enter only at the order  $\Lambda/m_b$ , whereas isospin-breaking in the form factors is expected to be a negligible effect. Therefore, the SM prediction is as small as  $O(5\%)$  (145, 148, 149, 150, 151). The ratio is especially sensitive to NP effects in the penguin sector, namely to the ratio of the two effective couplings  $C_6/C_7$ . The analogous isospin ratio in the  $\rho$  sector strongly depends on CKM parameters (150):

$$\Delta(\rho\gamma) = \frac{\Gamma(B^+ \rightarrow \rho^+\gamma)}{2\Gamma(B^0 \rightarrow \rho^0\gamma)} - 1 = (-4.6_{-4.2}^{+5.4}|_{\text{CKM}}^{+5.8}|_{\text{had}}) \times 10^{-2}. \quad (35)$$

The hadronic error is due mainly to the weak-annihilation contribution, to which a 50% error is assigned.

**$CP$  asymmetries in Radiative Decays** In the  $CP$  asymmetries, the uncertainties due to form factors cancel out to a large extent. But both the scale dependence and the dependence on the charm quark of the next-to-leading-order predictions are rather large because the  $CP$  asymmetries arise at  $O(\alpha_s)$  only. Although the direct  $CP$  asymmetry in  $B \rightarrow K^*\gamma$  is doubly Cabibbo suppressed and expected to be very small within the QCDF/SCET approach, one finds  $O(-10\%)$  predictions for the direct  $CP$  asymmetries in the  $B \rightarrow \rho\gamma$  mode (131, 148, 150). Because the weak-annihilation contribution does not contribute significantly here, the neutral and charged modes are of similar sizes (150):

$$\mathcal{A}_{CP}(\overline{B}^0 \rightarrow \rho^0\gamma) = (-10.4_{-2.4}^{+1.6}|_{\text{CKM}}^{+3.0}|_{\text{had}}) \% \quad (36)$$

and

$$\mathcal{A}_{CP}(B^- \rightarrow \rho^- \gamma) = (-10.7^{+1.5}_{-2.0} |_{\text{CKM}}^{+2.6} |_{\text{had}}) \% . \quad (37)$$

Finally, we reiterate that all predictions of exclusive observables within the QCDF/SCET approach may receive further uncertainties due to the unknown power corrections. This possibility might be especially important in the case of  $CP$  asymmetries.

The time-dependent  $CP$  asymmetry is given by two parameters,  $\mathcal{S}_{CP}$  and  $\mathcal{A}_{CP}$ :

$$\mathcal{A}_{CP}(B \rightarrow f; \Delta t) = \mathcal{S}_{CP} \sin(\Delta m \Delta t) + \mathcal{A}_{CP} \cos(\Delta m \Delta t), \quad (38)$$

where  $\mathcal{A}_{CP}$  represents the size of the direct  $CP$  asymmetry discussed above.<sup>4</sup> In hadronic decay modes such as  $B \rightarrow J/\psi K_S^0$ , a large value of  $\mathcal{S}_{CP}$  due to the angle  $\phi_1 \equiv \beta = -\arg(V_{td}V_{tb}^*/V_{ud}V_{ub}^*)$  of the unitarity triangle has been established, and a similarly large  $CP$  asymmetry is expected for hadronic penguin decays. This asymmetry is suppressed in radiative penguin decays because the photon helicities are opposite between those from  $B^0$  and  $\bar{B}^0$  decays under the left-handed current of SM weak decays, and they do not interfere in the limit of massless quarks. This finding implies a suppression factor of  $m_s/m_b$  in the leading contribution to  $\mathcal{S}_{CP}$  that is induced by the electromagnetic dipole operator  $\mathcal{O}_7$ :

$$\mathcal{S}_{CP}^{\text{SM}} = -\sin 2\phi_1 \frac{m_s}{m_b} [2 + O(\alpha_s)] + \mathcal{S}^{\text{SM},s\gamma g} \quad (39)$$

However, there are also additional contributions,  $\mathcal{S}^{\text{SM},s\gamma g}$  induced by the process  $b \rightarrow s\gamma g$  via operators other than  $\mathcal{O}_7$  (183,184). These corrections are not helicity-suppressed but are power-suppressed. A conservative dimensional estimate of the contribution from a nonlocal SCET operator series leads to  $|\mathcal{S}^{\text{SM},s\gamma g}| \approx 0.06$  (183,184), whereas within a QCD sum rule calculation, the contribution due to soft-gluon emission is estimated to be  $\mathcal{S}^{\text{SM},s\gamma g} = -0.005 \pm 0.01$  (185,151) which leads to  $\mathcal{S}_{CP}^{\text{SM}} = -0.022 \pm 0.015^{+0}_{-0.01}$ .<sup>5</sup> The QCD sum rule estimates of power corrections, namely long-distance contributions that arise from photon and soft-gluon emission from quark loops (151), lead to analogous results for the other radiative decay modes, such as  $B \rightarrow \rho \gamma$  (151). If a large value of  $\mathcal{S}_{CP}$  beyond the SM prediction is observed, it will signal a new right-handed current beyond the SM.

**$B \rightarrow K^* \ell^+ \ell^-$**  The isospin asymmetry in the mode  $B \rightarrow K^* \ell^+ \ell^-$ , as in the radiative mode, is a subleading  $\Lambda/m_b$  effect, but the dominant isospin-breaking effects can be calculated perturbatively, whereas other  $\Lambda/m_b$  corrections are simply estimated. Thus, the exact uncertainty is difficult to estimate due to unknown power corrections, but the observable may still be useful in the NP search because of its high sensitivity to specific Wilson coefficients (186).

The decay  $\bar{B}^0 \rightarrow \bar{K}^{*0} \ell^+ \ell^-$  (with  $\bar{K}^{*0} \rightarrow K^- \pi^+$  on the mass shell) is completely described by four independent kinematic variables: the lepton-pair invariant mass squared,  $q^2$ , and the three angles  $\theta_\ell$ ,  $\theta_K$ , and  $\phi$  (for their precise definitions, see

<sup>4</sup>The symbol  $\mathcal{C}_{CP} = -\mathcal{A}_{CP}$  is also often used.

<sup>5</sup>This does not necessarily contradict a larger time-dependent  $CP$  asymmetry of approximately 10% within the inclusive mode found in Ref. (183), because the SCET estimate (183,184) shows that the expansion parameter is  $\Lambda/Q$ . Here  $Q$  is the kinetic energy of the hadronic part. There is no contribution at leading order. Thus, the effect is expected to be larger for larger invariant hadronic mass. The  $K^*$  mode must have the smallest effect, below the average 10%.

Ref. (152, 187)). Summing over the spins of the final particles, the differential decay distribution can be written as (188, 189)

$$\frac{d^4\Gamma_{\overline{B}}}{dq^2 d\theta_\ell d\theta_K d\phi} = \frac{9}{32\pi} I(q^2, \theta_\ell, \theta_K, \phi) \sin\theta_\ell \sin\theta_K. \quad (40)$$

By integrating two of the angles, one finds

$$\frac{d\Gamma'}{d\theta_K} = \frac{3\Gamma'}{4} \sin\theta_K \left( 2F_L \cos^2\theta_K + (1 - F_L) \sin^2\theta_K \right), \quad (41)$$

and

$$\frac{d\Gamma'}{d\theta_\ell} = \Gamma' \left( \frac{3}{4} F_L \sin^2\theta_\ell + \frac{3}{8} (1 - F_L) (1 + \cos^2\theta_\ell) + A_{FB} \cos\theta_\ell \right) \sin\theta_\ell. \quad (42)$$

The observables appear linearly in the expressions so the fits can be performed on data binned in  $q^2$ . The fraction of longitudinal polarization  $F_L$  from the kaon angular distribution and the forward-backward asymmetry  $A_{FB}$  from the lepton angular distribution are accessible this way. The latter observable is defined as follows ( $\theta_\ell$  is defined below Eq. 25):

$$A_{FB}(q^2) \equiv \frac{1}{d\Gamma/dq^2} \left( \int_0^1 d(\cos\theta_\ell) \frac{d^2\Gamma}{dq^2 d\cos\theta_\ell} - \int_{-1}^0 d(\cos\theta_\ell) \frac{d^2\Gamma}{dq^2 d\cos\theta_\ell} \right). \quad (43)$$

The hadronic uncertainties of these two differential observables are large. However, the value of the dilepton invariant mass  $q_0^2$ , for which the differential forward-backward asymmetry vanishes, can be predicted in quite a clean way. In the QCDF approach at leading order in  $\Lambda/m_b$ , the value of  $q_0^2$  is free from hadronic uncertainties at order  $\alpha_s^0$ . A dependence on the soft form factor and on the light-cone wave functions of the  $B$  and  $K^*$  mesons appears only at order  $\alpha_s^1$ . At next-to-leading order one finds (150):

$$q_0^2[K^{*0}\ell^+\ell^-] = 4.36_{-0.31}^{+0.33} \text{ GeV}^2, \quad q_0^2[K^{*+}\ell^+\ell^-] = 4.15_{-0.27}^{+0.27} \text{ GeV}^2. \quad (44)$$

The small difference is due to isospin-breaking power corrections. However, an uncertainty due to unknown power corrections should be readded to the theoretical error bars. The zero is highly sensitive to the ratio of the two Wilson coefficients  $C_7$  and  $C_9$ . Thus, such a measurement would have a huge phenomenological impact.

In the near future, a full angular analysis based on the four-fold differential decay rate in Eq. 40 will become possible. Such rich information would allow for the design of observables with specific NP sensitivity and reduced hadronic uncertainties (152, 187). These observables would be constructed in such a way that the soft form factor dependence would cancel out at leading order for all dilepton masses, and they would have much higher sensitivity to new right-handed currents than would observables that are already accessible via the projection fits (189, 152, 187). In these optimized observables, the unknown  $\Lambda/m_b$  corrections would be the source of the largest uncertainty. Further detailed NP analyses of such angular observables have been presented in Refs. (191, 190). A full angular analysis provides high sensitivity to various Wilson coefficients, but the sensitivity to new weak phases is restricted (192, 187).

## 5 PRESENT EXPERIMENTAL RESULTS

The huge samples of  $B$  meson decays collected by Belle and BaBar have made it possible to fully explore the radiative penguin decays  $b \rightarrow s\gamma$  and  $b \rightarrow d\gamma$ , as well as the electroweak penguin decays  $b \rightarrow s\ell^+\ell^-$ .

### 5.1 Inclusive $B \rightarrow X_s\gamma$ Branching Fraction

An experimental challenge is how to lower the minimum photon energy to 1.6 GeV (see Section 2.4). Before the construction of the  $B$  factories, minimum photon energy of 2.0 GeV was required in the measurement by CLEO (193). BaBar has a minimum photon-energy requirement of 1.9 GeV based on 89 million  $B\bar{B}$  pairs (194), whereas Belle first reported the result of 1.8 GeV with 152 million  $B\bar{B}$  pairs (195). Belle recently lowered the limit to 1.7 GeV by using 657 million  $B\bar{B}$  pairs (196) (Fig. 5). Belle measured the branching fraction to be  $\mathcal{B}(B \rightarrow X_s\gamma) = (345 \pm 15 \pm 40) \times 10^{-6}$  for  $E_\gamma > 1.7$  GeV, whereas BaBar measured it to be  $(367 \pm 29 \pm 34 \pm 29) \times 10^{-6}$  for  $E_\gamma > 1.9$  GeV.

The sum-of-exclusive technique and the  $B$ -reco technique have been used by BaBar with a minimum photon-energy requirement of 1.9 GeV (197, 198), which corresponds to a maximum recoil mass requirement of 2.8 GeV. Belle also made a sum-of-exclusive measurement using a very early data set (199).

To calculate the average branching fraction based on the same phase space and to compare it with theory predictions, the Heavy Flavor Averaging Group (HFAG) (200) has made an extrapolation of the branching fraction to the same minimum photon energy of 1.6 GeV (116). The extrapolation factor is 0.985  $\pm$  0.004 ( $0.894 \pm 0.016$ ) for 1.7 (2.0) GeV. The average thereby obtained is

$$\mathcal{B}(B \rightarrow X_s\gamma) = (352 \pm 23 \pm 9) \times 10^{-6}, \quad (45)$$

where the first error is statistical and systematic combined, and the second is due to the extrapolation. The result is in agreement with the SM prediction given in Eq. 17, and it provides stringent constraints on NP, as discussed in Section 4.1.

### 5.2 Exclusive Measurements of $b \rightarrow s\gamma$ Processes

The recoil system of  $B \rightarrow X_s\gamma$  below 1.1 GeV is dominated by the  $K^*$  resonance, as the spin-0 state is forbidden. Above 1.1 GeV,  $X_s$  is a mixture of various resonant and nonresonant states and therefore can usually be modeled as a continuum spectrum in the inclusive  $B \rightarrow X_s\gamma$  analysis. The  $K^*$  signal makes it possible to use the channel for various studies, as discussed below. The  $B \rightarrow K^*\gamma$  branching fractions have been measured precisely by Belle (201) and BaBar (154) and have been averaged by HFAG to be

$$\begin{aligned} \mathcal{B}(B^0 \rightarrow K^{*0}\gamma) &= (43.3 \pm 1.5) \times 10^{-6} \\ \mathcal{B}(B^+ \rightarrow K^{*+}\gamma) &= (42.1 \pm 1.8) \times 10^{-6}, \end{aligned} \quad (46)$$

which corresponds to approximately 12% of the total  $B \rightarrow X_s\gamma$  branching fraction. The SM predictions for the branching fraction have been calculated by many groups. They are consistent with the measured values but have very large errors of 30% to 50%, which arise mainly from the uncertainty of the  $B \rightarrow K^*$  form factor (130, 131).



The resonant structure of the high mass  $X_s$  system has also been explored. So far,  $B \rightarrow K_2^*(1430)\gamma$  (202, 203) and  $B \rightarrow K_1(1270)\gamma$  (204) have been measured, but other decay channels such as  $B \rightarrow K_1(1400)\gamma$  seem to have small branching fractions and have not yet been observed. In addition, many multi-body final states have been measured, such as  $B \rightarrow K\pi\pi\gamma$  (205, 202) (including  $B \rightarrow K^*\pi\gamma$  and  $B \rightarrow K\rho\gamma$ ),  $B \rightarrow K\phi\gamma$  (206, 207),  $B \rightarrow K\eta\gamma$  (208, 209),  $B \rightarrow K\eta'\gamma$  (210), and  $B \rightarrow \Lambda\bar{p}\gamma$  (211).

### 5.3 $CP$ and Isospin Asymmetries in $b \rightarrow s\gamma$ Processes

The measurement of the inclusive direct  $CP$  asymmetry (Eq. 20) was performed by use of the sum-of-exclusive method to tag the flavor of the  $B$  candidate. For  $B^0$  ( $\bar{B}^0$ ), only the self-tagging modes with a  $K^+$  ( $K^-$ ) were used. The measured asymmetry was corrected for a small dilution due to the doubly misidentified pair of a charged kaon and a pion. The results, based on 152 and 383 million  $B\bar{B}$  samples by Belle and BaBar, are  $0.002 \pm 0.050 \pm 0.030$  (212) and  $-0.011 \pm 0.030 \pm 0.014$  (213), respectively, and have been averaged by HFAG to be

$$\mathcal{A}_{CP}(\bar{B} \rightarrow X_s\gamma) = -0.012 \pm 0.028. \quad (47)$$

This is consistent with null asymmetry, and the size of the error is still much larger than the SM precision (Eq. 21). Assuming the systematic error can be reduced along with the statistical error, a data set two orders of magnitude larger would be more sensitive to NP, although still insufficient to measure the small  $\mathcal{A}_{CP}$  predicted by the SM.

In the exclusive  $B \rightarrow K^*\gamma$  channel, the direct  $CP$  asymmetry is also small but has less-understood theoretical uncertainties. Experimentally it can be measured more precisely. The current HFAG average is

$$\mathcal{A}_{CP}(B \rightarrow K^*\gamma) = -0.003 \pm 0.017, \quad (48)$$

which is also consistent with null asymmetry.

In the fully inclusive measurement, flavor information is not available for the signal side, but it can be obtained from the charge of the lepton in the event if the other  $B$  decays into a semileptonic final state. In this case, it is not possible to discriminate  $B \rightarrow X_d\gamma$  from  $B \rightarrow X_s\gamma$  and the measured asymmetry corresponds to a combined one. This combined asymmetry (note the different normalization in comparison with Eq. 24) has been measured by BaBar to be

$$\mathcal{A}_{CP}(B \rightarrow X_{s+d}\gamma) = -0.110 \pm 0.115 \pm 0.017, \quad (49)$$

which is consistent with null asymmetry but has a much larger error than do the other two asymmetry measurements.

The measurement of the isospin asymmetry (Eq. 34) is another way to utilize the reconstructed  $B \rightarrow K^*\gamma$  events. Here, the measured branching fractions are corrected by the lifetime ratio:  $\tau_{B^+}/\tau_{B^0} = 1.071 \pm 0.009$  (214). Usually  $B$  decay branching fractions are quoted based on the assumption of  $\mathcal{B}(\Upsilon(4S) \rightarrow B^+B^-) = \mathcal{B}(\Upsilon(4S) \rightarrow B^0\bar{B}^0) = 0.5$ , but the isospin-asymmetry measurement is already precise enough to be affected by the difference in these branching fractions. Belle measures  $\Delta_{0+}(B \rightarrow K^*\gamma) = 0.012 \pm 0.044 \pm 0.026$  without this correction, whereas BaBar measures  $\Delta_{0+}(B \rightarrow K^*\gamma) = 0.066 \pm 0.021 \pm 0.022$  using  $\mathcal{B}(\Upsilon(4S) \rightarrow B^+B^-) = 0.516 \pm 0.006$  and  $\mathcal{B}(\Upsilon(4S) \rightarrow B^0\bar{B}^0) = 0.484 \pm 0.006$  (214). After

scaling the Belle result and including the CLEO result using the aforementioned lifetime and production ratios, the naïve world average is

$$\Delta_{0+}(B \rightarrow K^*\gamma) = 0.062 \pm 0.027. \quad (50)$$

This average is in agreement with the SM expectation.

A similar isospin asymmetry can be also measured for the inclusive  $B \rightarrow X_s\gamma$  decay by use of the sum-of-exclusive method. The result by BaBar is

$$\Delta_{0+}(B \rightarrow X_s\gamma) = -0.006 \pm 0.058 \pm 0.009 \pm 0.024, \quad (51)$$

which is consistent with null asymmetry but is not yet as precise as that for  $B \rightarrow K^*\gamma$ .

The measurement of the time-dependent  $CP$  asymmetry (Eq. 38) for  $b \rightarrow s\gamma$  faces two experimental challenges. First, the modes and statistics that can be used for time-dependent  $CP$  asymmetry measurements are rather limited. Although the  $B^0 \rightarrow K^{*0}\gamma$  branching fraction is not very small, only 1/9 of the events that decay into the  $K_S^0(\rightarrow \pi^+\pi^-)\pi^0\gamma$  final state can be used. Second, the  $B$  meson decay vertex position has to be extrapolated from the displaced  $K_S^0 \rightarrow \pi^+\pi^-$  vertex and the  $K_S^0$  momentum vector. Therefore, the  $K_S^0$  decays inside the vertex detector volume (55% in Belle, 68% in BaBar) and the resulting vertex resolution is somewhat degraded.

Because any  $B \rightarrow P^0Q^0\gamma$  final states [where  $P^0$  and  $Q^0$  are  $CP$  eigenstates (215)] can be used, the  $B \rightarrow K_S^0\pi^0\gamma$  events with  $M_{K_S^0\pi^0}$  up to 1.8 GeV including  $K_2^*(1430)$  were measured by both Belle (216) and BaBar (217) and have been averaged by HFAG as

$$\mathcal{S}_{CP}(B \rightarrow K_S^0\pi^0\gamma) = -0.15 \pm 0.20, \quad (52)$$

in which the  $B^0 \rightarrow K^{*0}\gamma$  contribution gives  $\mathcal{S}_{CP}(B \rightarrow K^*\gamma) = -0.16 \pm 0.22$ .

As additional channels, BaBar has measured  $\mathcal{S}_{CP}(B \rightarrow K_S^0\eta\gamma) = -0.18^{+0.49}_{-0.46} \pm 0.12$  (209), and Belle has measured  $\mathcal{S}_{CP}(B \rightarrow K_S^0\rho^0\gamma) = 0.11 \pm 0.33^{+0.05}_{-0.09}$  (218). The latter is slightly diluted by the  $B \rightarrow K^{*+}\pi^-\gamma$  events, by a factor which was measured to be  $0.83^{+0.19}_{-0.03}$ , but is free from the restriction of  $K_S^0$  vertexing and has a statistical error comparable in size to that of the  $B \rightarrow K_S^0\pi^0\gamma$  mode. Currently all results are compatible with null asymmetry with errors that are still not small enough to provide nontrivial constraints on right-handed currents, but this observable will be one of the best ways to search for NP in future experiments.

#### 5.4 Measurements of $b \rightarrow d\gamma$ Processes

Three exclusive  $b \rightarrow d\gamma$  decay modes are considered to be the easiest modes to study the  $b \rightarrow d\gamma$  process:  $B^+ \rightarrow \rho^+\gamma$ ,  $B^0 \rightarrow \rho^0\gamma$  and  $B^0 \rightarrow \omega\gamma$ . Although these modes have been searched for since the beginning of Belle and BaBar, only in the later stage of these experiments were measurements of the  $B \rightarrow \rho\gamma$  modes established. This is partly because of the large  $B \rightarrow K^*\gamma$  background and partly due to the huge continuum background, which is more severe for modes without a kaon in the final state. Therefore, large statistics and good particle identification are essential; Belle has the advantage in the former, whereas BaBar leads in the latter.

To gain statistics, these three modes have been combined by assuming their naïve quark contents, through the use of  $\Gamma(B^+ \rightarrow \rho^+\gamma) = 2\Gamma(B^0 \rightarrow \rho^0\gamma) =$

$2\Gamma(B^0 \rightarrow \omega\gamma)$ . In the latest measurements by both Belle (219) and BaBar (220), the  $B^0 \rightarrow \rho^0\gamma$  mode was measured with more than  $5\sigma$  significance and  $B^+ \rightarrow \rho^+\gamma$  with more than  $3\sigma$  significance, whereas  $B^0 \rightarrow \omega\gamma$  remains unestablished with significance less than  $3\sigma$ . Using the symbol  $B \rightarrow (\rho, \omega)\gamma$  for the combined results that are adjusted for the  $B^+ \rightarrow \rho^+\gamma$  mode, the averaged branching fraction by HFAG becomes

$$\mathcal{B}(B \rightarrow (\rho, \omega)\gamma) = (1.30_{-0.19}^{+0.18}) \times 10^{-6}. \quad (53)$$

The results are consistent with the SM predictions. However, these predictions are affected by form factor uncertainties and do not have effective prediction power for NP.

A more effective way to use these results is to combine them with the  $B \rightarrow K^*\gamma$  measurements to determine  $|V_{td}/V_{ts}|$ . Using Eq. 31, Belle and BaBar reported the value of  $|V_{td}/V_{ts}|$  to be  $0.195_{-0.019}^{+0.020} \pm 0.015$  and  $0.233_{-0.024}^{+0.025} {}_{-0.021}^{+0.022}$ , respectively, where the errors are experimental and theoretical. These results from the penguin diagrams are in agreement with the determination from the box diagrams using the ratio of the  $B^0$  and  $B_s^0$  mixing parameters  $\Delta m_d/\Delta m_s$ , where  $\Delta m_d$  is measured at the  $B$  factories and  $\Delta m_s$  at the Tevatron. The results are also in agreement with the more indirect determination by the unitarity triangle fit from other observables. This is a nontrivial test of the CKM scheme. However, although the experimental errors are still larger than the theoretical errors, the size of the theoretical error is unlikely to be reduced.

A possible way to improve this situation utilizes the inclusive  $B \rightarrow X_d\gamma$  measurement with the sum-of-exclusive method. BaBar has reconstructed the  $X_d\gamma$  system in seven final states ( $\pi^+\pi^-\gamma$ ,  $\pi^+\pi^0\gamma$ ,  $\pi^+\pi^-\pi^+\gamma$ ,  $\pi^+\pi^-\pi^0\gamma$ ,  $\pi^+\pi^-\pi^+\pi^-\gamma$ ,  $\pi^+\pi^-\pi^+\pi^0\gamma$ ,  $\pi^+\eta\gamma$ ) (221) in the mass range  $0.6 < M_{X_d} < 1.8$  GeV, which covers approximately 50% of the total branching fraction. To reduce the uncertainty due to missing modes and phase space,  $X_s\gamma$  modes were also measured in the corresponding seven final states in the same mass range, where the first  $\pi^+$  was replaced with  $K^+$ . The ratio of the two inclusive branching fractions is

$$\frac{\mathcal{B}(B \rightarrow X_d\gamma)}{\mathcal{B}(B \rightarrow X_s\gamma)} = 0.033 \pm 0.013 \pm 0.009, \quad (54)$$

which is converted to  $|V_{td}/V_{ts}| = 0.177 \pm 0.043 \pm 0.001$ , where the theory error does not include the effect due to the limited mass range. This result is also in good agreement with other determinations.

The direct  $CP$  asymmetry for  $B \rightarrow \rho\gamma$  can be as large as  $\sim -10\%$  in the SM, whereas the time-dependent  $CP$  asymmetry is doubly suppressed due to the photon helicity and the cancellation of the CKM element  $V_{td}$ . The latter appears in the mixing and in the  $b \rightarrow d$  penguin decay. However, the  $\rho^0 \rightarrow \pi^+\pi^-$  decay provides clear vertex information for  $B^0 \rightarrow \rho^0\gamma$ . Both  $CP$  asymmetries have been measured by Belle (219, 222) as

$$\begin{aligned} \mathcal{A}_{CP}(B^+ \rightarrow \rho^+\gamma) &= -0.11 \pm 0.32 \pm 0.09, \\ \mathcal{A}_{CP}(B^0 \rightarrow \rho^0\gamma) &= -0.44 \pm 0.49 \pm 0.14, \text{ and} \\ \mathcal{S}_{CP}(B^0 \rightarrow \rho^0\gamma) &= -0.83 \pm 0.65 \pm 0.18. \end{aligned} \quad (55)$$

So far the results are consistent with null asymmetry. A nonzero direct  $CP$  violation may be measured earlier in  $B \rightarrow \rho\gamma$  than in  $B \rightarrow K^*\gamma$ .

The isospin asymmetry (Eq. 35) is also expected to be as large as  $\sim -5\%$  in  $B \rightarrow \rho\gamma$ . Belle measures  $\Delta(\rho\gamma) = -0.48_{-0.19}^{+0.21} {}_{-0.09}^{+0.08}$  (219), and BaBar mea-

sures  $\Delta(\rho\gamma) = -0.43_{-0.22}^{+0.25} \pm 0.10$  (220); both measurements show a large isospin asymmetry. The average by HFAG is

$$\Delta(\rho\gamma) = -0.46_{-0.16}^{+0.17}. \quad (56)$$

A significant nonzero isospin asymmetry could indicate NP.

### 5.5 Exclusive $B \rightarrow K^{(*)}\ell^+\ell^-$ Branching Fraction

Despite their small branching fractions, the exclusive decay channels  $B \rightarrow K^{(*)}\ell^+\ell^-$  have been measured efficiently with small background at Belle and BaBar, given that their final states are the same as those of  $B \rightarrow J/\psi K^{(*)}$  for which the  $B$  factories were designed. Here,  $K^{(*)}$  is one of  $K^+$ ,  $K_S^0$ ,  $K^{*+}$  and  $K^{*0}$ , and  $\ell^+\ell^-$  is either  $e^+e^-$  or  $\mu^+\mu^-$ .

Electrons are identified by their energy deposit through an electromagnetic shower in the calorimeter. The minimum momentum is required to be greater than 0.4 GeV by Belle or 0.5 GeV by BaBar. The momentum of the bremsstrahlung photons that may be emitted by the electrons are added to their momenta if they are found near the electron direction. Muons have to reach and penetrate into the outer muon detectors and the minimum momentum is required to be 0.7 GeV by Belle or 1.0 GeV by BaBar. The dilepton mass regions around  $J/\psi$  and  $\psi(2S)$  are vetoed.

The branching fractions, averaged over the lepton and kaon flavors and integrated over the dilepton masses, assuming the SM distribution over the vetoed  $J/\psi$  and  $\psi(2S)$ , were measured by Belle (223) and BaBar (224) and have been averaged by HFAG as

$$\begin{aligned} \mathcal{B}(B \rightarrow K\ell^+\ell^-) &= (4.5 \pm 0.4) \times 10^{-7}, \\ \mathcal{B}(B \rightarrow K^*\ell^+\ell^-) &= (10.8_{-1.1}^{+1.2}) \times 10^{-7}. \end{aligned} \quad (57)$$

The results are consistent with SM expectations. At present, the irreducible form factor uncertainty in the SM calculations prevents these results from placing meaningful constraints on NP.

A small subset of these combinations,  $B^+ \rightarrow K^+\mu^+\mu^-$  and  $B^0 \rightarrow K^{*0}\mu^+\mu^-$ , can be efficiently measured at hadron colliders. CDF has reported the most precise measurements of these modes (225).

### 5.6 $B \rightarrow K^{(*)}\ell^+\ell^-$ Asymmetries and Angular Distributions

The direct  $CP$  and isospin asymmetries in  $B \rightarrow K^{(*)}\ell^+\ell^-$  are also useful in the search for NP. The direct  $CP$  asymmetries are consistent with null values,  $\mathcal{A}_{CP}(B \rightarrow K^+\ell^+\ell^-) = -0.01 \pm 0.09$  and  $\mathcal{A}_{CP}(B \rightarrow K^*\ell^+\ell^-) = -0.07 \pm 0.08$  as averaged by HFAG. However, nonzero negative isospin asymmetries in the small  $q^2$ -region of  $B \rightarrow K\ell^+\ell^-$  ( $3.2\sigma$ ) and  $B \rightarrow K^*\ell^+\ell^-$  ( $2.7\sigma$ ) have been reported by BaBar ( $3.9\sigma$  when combined). The corresponding isospin asymmetries by Belle are  $1.4\sigma$  and  $1.8\sigma$  from zero, and are consistent with both BaBar's results and null asymmetry. The isospin asymmetry combined for  $B \rightarrow K^{(*)}\ell^+\ell^-$  and averaged by HFAG is

$$A_I^{K^{(*)}} = -0.45 \pm 0.10. \quad (58)$$

The SM prediction is essentially zero at this level of statistics (see Section 4.2).

Muon to electron ratios in  $B \rightarrow K^{(*)}\ell^+\ell^-$  (Eq. 30) are also measured by both Belle and BaBar. Results are consistent with the SM, and their naïve averages are  $R_K = 1.02 \pm 0.18$  and  $R_{K^*} = 0.88 \pm 0.17$ .

The four-body decay configuration of  $B \rightarrow K^*\ell^+\ell^- \rightarrow K\pi\ell^+\ell^-$  allows extraction of further information from the angular distributions of the final-state particles. The most interesting observables are the fraction of longitudinal polarization  $F_L$  from the kaon angular distribution (Eq. 41) and the forward-backward asymmetry  $A_{FB}$  from the lepton angular distribution (Eq. 42). Belle has measured  $F_L$  and  $A_{FB}$  in six bins of  $q^2$  (223), whereas BaBar has done so in two bins (226). Current statistics are not enough to tell whether there is a zero-crossing point at low  $q^2$ , although the results favor the case with no crossing, for which the sign of the Wilson coefficient  $C_7$  is flipped. Both results have positive  $A_{FB}$  for high  $q^2$  (Fig. 6), which sets nontrivial constraints on the Wilson coefficients. CDF has also measured  $F_L$  and  $A_{FB}$  in the same six bins as Belle for  $B^0 \rightarrow K^{*0}\mu^+\mu^-$  events (225). The results are in agreement with Belle and BaBar.

### 5.7 Inclusive $B \rightarrow X_s\ell^+\ell^-$ Branching Fraction

The inclusive  $B \rightarrow X_s\ell^+\ell^-$  branching fraction has been measured by Belle and BaBar using the sum-of-exclusive technique. The  $X_s$  system includes final states with one kaon and up to four (two) pions that have masses up to 2.0 (1.8) GeV for the result by Belle (BaBar). Belle recently announced a preliminary result based on 657 million  $B\bar{B}$  (227), and BaBar's result is based on 89 million  $B\bar{B}$  (228). In Belle's new analysis, partial branching fractions are measured in bins of the  $X_s$  mass, and then the total branching fraction is calculated as their sum. This method reduces the large systematic error observed in previous studies that arose from the strong  $X_s$  mass dependence of the efficiency and the unknown fractions of exclusive channels  $B \rightarrow K^{(*)}\ell^+\ell^-$ . The measurement is still dominated by the statistical error and will be more precise in the future. Belle and BaBar reported branching fractions as  $\mathcal{B}(B \rightarrow X_s\ell^+\ell^-) = (3.33 \pm 0.80^{+0.19}_{-0.24}) \times 10^{-6}$  and  $\mathcal{B}(B \rightarrow X_s\ell^+\ell^-) = (5.6 \pm 1.5 \pm 0.6 \pm 1.1) \times 10^{-6}$ , respectively, which were averaged by HFAG as

$$\mathcal{B}(B \rightarrow X_s\ell^+\ell^-) = (3.66^{+0.76}_{-0.77}) \times 10^{-6}, \quad (59)$$

integrated over the entire subset of phase space with  $q^2 > 0.2$  GeV, including the vetoed  $J/\psi$  and  $\psi(2S)$  regions. The results are in good agreement with the SM prediction. They strongly disfavor the case with the flipped sign of  $C_7$  (179).

## 6 OUTLOOK

Remarkably, the  $B$  factories have measured all the observables within the radiative and electroweak penguin decays at values that are consistent with the SM predictions. These measurements rule out  $O(1)$  corrections to the SM and identify the CKM theory as the dominant effect for flavor violation as well as for  $CP$  violation. The success of the simple CKM theory of  $CP$  violation was honored with the Nobel Prize in Physics in 2008. Theoretical tools and precision have significantly advanced during the past decade, and we are ready to challenge the SM if a clear deviation is found or to discriminate different NP scenarios if direct evidence is found at the LHC.

Also, the future offers great experimental opportunities in flavor physics. LHCb has finally started taking data and promises to overwhelm many  $B$  factory results, and ATLAS and CMS will also contribute to flavor physics. In the radiative and electroweak penguin decays, the most promising measurements are the angular analysis of  $B^0 \rightarrow K^{*0} \mu^+ \mu^-$  and the analysis of time-dependent  $CP$  asymmetry in  $B_s \rightarrow \phi \gamma$ ; the latter measurement cannot be performed at the  $B$  factories due to the fast  $B_s$  oscillation. However, the theoretically clean inclusive modes and many modes involving neutral particles like the  $\pi^0$  can be pursued only at the  $e^+e^-$   $B$  factories. Two proposed super- $B$  factories, Belle II at KEK and SuperB in Italy, would accumulate two-orders-of-magnitude-larger data samples. Such data would push experimental precision to its limit.

Theoretical and experimental techniques are ready for such large data samples. The results provided by LHCb and the next-generation  $e^+e^-$   $B$  factories are eagerly awaited, as they may be the key to identifying physics beyond the SM.

## ACKNOWLEDGMENTS

We thank Christoph Greub, Colin Jessop, and Kurtis Nishimura for their careful reading of the manuscript, and Thorsten Feldmann, Matthias Neubert, and Gil Paz for comments. T.H. thanks the CERN Theory Group for its hospitality during his visits to CERN.

## LITERATURE CITED

1. Ellis JR, Gaillard MK, Nanopoulos DV, Rudaz S. *Nucl. Phys. B* 131:285 (1977), *Erratum-ibid.* 132:541 (1978)
2. Shifman MA. arXiv:hep-ph/9510397 (1995)
3. Belle collaboration: <http://belle.kek.jp/>
4. BaBar collaboration: <http://www.slac.stanford.edu/BFROOT/>
5. Kobayashi M, Maskawa T. *Prog. Theor. Phys.* 49:652 (1973)
6. Cabibbo N. *Phys. Rev. Lett.* 10:531 (1963)
7. CDF collaboration:  
<http://www-cdf.fnal.gov/physics/new/bottom/bottom.html>
8. D0 collaboration:  
<http://www-d0.fnal.gov/Run2Physics/WWW/results/b.htm>
9. Artuso M, et al. *Eur. Phys. J. C* 57:309 (2008), arXiv:0801.1833 [hep-ph]
10. Antonelli M, et al. arXiv:0907.5386 [hep-ph] (2009)
11. Isidori G, Nir Y, Perez G. in the same volume of *Ann. Rev. Nucl. Part. Sci.* (2010), arXiv:1002.0900 [hep-ph]
12. Buras AJ. arXiv:0910.1032 [hep-ph] (2009)
13. Ammer R, et al. (CLEO Collab.) *Phys. Rev. Lett.* 71:674 (1993)
14. Alam MS, et al. (CLEO Collab.) *Phys. Rev. Lett.* 74:2885 (1995)
15. Lingel K, Skwarnicki T, Smith JG. *Ann. Rev. Nucl. Part. Sci.* 48:253 (1998)
16. Hurth T. *Rev. Mod. Phys.* 75:1159 (2003), arXiv:hep-ph/0212304
17. Hurth T, Lunghi E. *In the Proceedings of 2nd Workshop on the CKM Unitarity Triangle, Durham, England, 5-9 Apr 2003*, arXiv:hep-ph/0307142
18. Hurth T. *Int. J. Mod. Phys. A* 22:1781 (2007), arXiv:hep-ph/0703226
19. Wilson KG. *Phys. Rev.* 179:1499 (1969)
20. Wilson KG. *Phys. Rev. D* 3:1818 (1971)

21. Gaillard MK, Lee BW. *Phys. Rev. Lett.* 33:108 (1974)
22. Altarelli G, Maiani L. *Phys. Lett. B* 52:351 (1974)
23. Witten E. *Nucl. Phys. B* 122:109 (1977)
24. Chay J, Georgi H, Grinstein B. *Phys. Lett. B* 247:399 (1990)
25. Bigi II, Uraltsev NG, Vainshtein AI. *Phys. Lett. B* 293:430 (1992),  
*Erratum-ibid* 297:477 (1993), arXiv:hep-ph/9207214
26. Bigi II, et al. arXiv:hep-ph/9212227 (1992)
27. Bigi II, Shifman MA and Uraltsev N. *Ann. Rev. Nucl. Part. Sci.* 47:591 (1997), arXiv:hep-ph/9703290
28. Manohar AV and Wise MB. *Phys. Rev. D* 49:1310 (1994),  
arXiv:hep-ph/9308246
29. Manohar AV, Wise MB. *Camb. Monogr. Part. Phys. Nucl. Phys. Cosmol.* 10:1 (2000)
30. Falk AF, Luke ME, Savage MJ. *Phys. Rev. D* 49:3367 (1994),  
arXiv:hep-ph/9308288
31. Ali A, Hiller G, Handoko LT, Morozumi T. *Phys. Rev. D* 55:4105 (1997),  
arXiv:hep-ph/9609449
32. Beneke M, Buchalla G, Neubert M, Sachrajda CT. *Phys. Rev. Lett.* 83:1914 (1999), arXiv:hep-ph/9905312
33. Beneke M, Buchalla G, Neubert M, Sachrajda CT. *Nucl. Phys. B* 591:313 (2000), arXiv:hep-ph/0006124
34. Beneke M, Buchalla G, Neubert M, Sachrajda CT. *Nucl. Phys. B* 606:245 (2001), arXiv:hep-ph/0104110
35. Bauer CW, Fleming S, Luke ME. *Phys. Rev. D* 63:014006 (2000),  
arXiv:hep-ph/0005275
36. Bauer CW, Fleming S, Pirjol D, Stewart IW. *Phys. Rev. D* 63:114020 (2001), arXiv:hep-ph/0011336
37. Bauer CW, Stewart IW. *Phys. Lett. B* 516:134 (2001),  
arXiv:hep-ph/0107001
38. Bauer CW, Pirjol D, Stewart IW. *Phys. Rev. D* 65:054022 (2002),  
arXiv:hep-ph/0109045
39. Beneke M, Chapovsky AP, Diehl M, Feldmann T. *Nucl. Phys. B* 643:431 (2002), arXiv:hep-ph/0206152
40. Hill RJ, Neubert M. *Nucl. Phys. B* 657:229 (2003), arXiv:hep-ph/0211018
41. Ciuchini M et al. *Phys. Lett. B* 316:127 (1993), arXiv:hep-ph/9307364
42. Ciuchini M, Franco E, Martinelli G, Reina L. *Nucl. Phys. B* 415:403 (1994),  
arXiv:hep-ph/9304257
43. Cella G, Curci G, Ricciardi G, Vicere A. *Nucl. Phys. B* 431:417 (1994),  
arXiv:hep-ph/9406203
44. Misiak M. *Nucl. Phys. B* 393:23 (1993), *Erratum-ibid* 439:461 (1995)
45. Adel K, Yao YP. *Phys. Rev. D* 49:4945 (1994), arXiv:hep-ph/9308349
46. Greub C, Hurth T. *Phys. Rev. D* 56:2934 (1997), arXiv:hep-ph/9703349
47. Chetyrkin KG, Misiak M, Munz M. *Phys. Lett. B* 400:206 (1997),  
*Erratum-ibid* 425:414 (1998), arXiv:hep-ph/9612313
48. Gambino P, Gorbahn M, Haisch U. *Nucl. Phys. B* 673:238 (2003),  
arXiv:hep-ph/0306079
49. Ali A, Greub C. *Z. Phys. C* 49:431 (1991)
50. Greub C, Hurth T, Wyler D. *Phys. Rev. D* 54:3350 (1996),  
arXiv:hep-ph/9603404
51. Pott N. *Phys. Rev. D* 54:938 (1996), arXiv:hep-ph/9512252

52. Buras AJ, Czarnecki A, Misiak M, Urban J. *Nucl. Phys. B* 611:488 (2001), arXiv:hep-ph/0105160
53. Buras AJ, Czarnecki A, Misiak M, Urban J. *Nucl. Phys. B* 631:219 (2002), arXiv:hep-ph/0203135
54. Gambino P, Misiak M. *Nucl. Phys. B* 611:338 (2001), arXiv:hep-ph/0104034
55. Hurth T, Lunghi E, Porod W. *Nucl. Phys. B* 704:56 (2005), arXiv:hep-ph/0312260
56. Hurth T, Lunghi E, Porod W. *Eur. Phys. J. C* 33:s382 (2004), arXiv:hep-ph/0310282
57. Asatrian HM et al. *Phys. Lett. B* 619:322 (2005), arXiv:hep-ph/0505068
58. Misiak M, et al. *Phys. Rev. Lett.* 98:022002 (2007), arXiv:hep-ph/0609232
59. Misiak M, Steinhauser M. *Nucl. Phys. B* 683:277 (2004), arXiv:hep-ph/0401041
60. Bobeth C, Misiak M, Urban J. *Nucl. Phys. B* 574:291 (2000), arXiv:hep-ph/9910220
61. Gorbahn M, Haisch U. *Nucl. Phys. B* 713:291 (2005), arXiv:hep-ph/0411071
62. Gorbahn M, Haisch U, Misiak M. *Phys. Rev. Lett.* 95:102004 (2005), arXiv:hep-ph/0504194
63. Czakon M, Haisch U, Misiak M. *JHEP* 0703:008 (2007), arXiv:hep-ph/0612329
64. Melnikov K, Mitov A. *Phys. Lett. B* 620:69 (2005), arXiv:hep-ph/0505097
65. Blokland I et al. *Phys. Rev. D* 72:033014 (2005), arXiv:hep-ph/0506055
66. Asatrian HM, et al. *Nucl. Phys. B* 749:325 (2006), arXiv:hep-ph/0605009
67. Asatrian HM, et al. *Nucl. Phys. B* 762:212 (2007), arXiv:hep-ph/0607316
68. Bieri K, Greub C, Steinhauser M. *Phys. Rev. D* 67:114019 (2003), arXiv:hep-ph/0302051
69. Misiak M, Steinhauser M. *Nucl. Phys. B* 764:62 (2007), arXiv:hep-ph/0609241
70. Boughezal R, Czakon M, Schutzmeier T, *JHEP* 0709:072 (2007), arXiv:0707.3090 [hep-ph]
71. Ligeti Z, Luke ME, Manohar AV, Wise MB. *Phys. Rev. D* 60:034019 (1999), arXiv:hep-ph/9903305
72. Asatrian HM, Ewerth T, Gabrielyan H, Greub C. *Phys. Lett. B* 647:173 (2007), arXiv:hep-ph/0611123
73. Ewerth T. *Phys. Lett. B* 669:167 (2008), arXiv:0805.3911 [hep-ph]
74. Czarnecki A, Marciano WJ. *Phys. Rev. Lett.* 81:277 (1998), arXiv:hep-ph/9804252
75. Kagan AL, Neubert M. *Eur. Phys. J. C* 7:5 (1999), arXiv:hep-ph/9805303
76. Baranowski K, Misiak M. *Phys. Lett. B* 483:410 (2000), arXiv:hep-ph/9907427
77. Gambino P, Haisch U. *JHEP* 0110:020 (2001), arXiv:hep-ph/0109058
78. Buras AJ, Munz M. *Phys. Rev. D* 52:186 (1995), arXiv:hep-ph/9501281
79. Asatryan HH, Asatrian HM, Greub C, Walker M. *Phys. Rev. D* 65:074004 (2002), arXiv:hep-ph/0109140
80. Asatryan HH, Asatrian HM, Greub C, Walker M. *Phys. Rev. D* 66:034009 (2002), arXiv:hep-ph/0204341
81. Ghinculov A, Hurth T, Isidori G, Yao YP. *Nucl. Phys. B* 685:351 (2004), arXiv:hep-ph/0312128
82. Ghinculov A, Hurth T, Isidori G, Yao YP. *Eur. Phys. J. C* 33:s288 (2004), arXiv:hep-ph/0310187



83. Asatrian HM, Bieri K, Greub C, Hovhannisyanyan A. *Phys. Rev. D* 66:094013 (2002), arXiv:hep-ph/0209006
84. Asatrian HM, Asatryan HH, Hovhannisyanyan A, Poghosyan V. *Mod. Phys. Lett. A* 19:603 (2004), arXiv:hep-ph/0311187
85. Ghinculov A, Hurth T, Isidori G, Yao YP. *Nucl. Phys. B* 648:254 (2003), arXiv:hep-ph/0208088
86. Greub C, Pilipp V, Schupbach C. *JHEP* 0812:040 (2008), arXiv:0810.4077 [hep-ph]
87. Huber T, Hurth T, Lunghi E. arXiv:0807.1940 [hep-ph] (2008)
88. Bobeth C, Gambino P, Gorbahn M, Haisch U. *JHEP* 0404:071 (2004), arXiv:hep-ph/0312090
89. Huber T, Lunghi E, Misiak M, Wyler D. *Nucl. Phys. B* 740:105 (2006), arXiv:hep-ph/0512066
90. Huber T, Hurth T, Lunghi E. *Nucl. Phys. B* 802:40 (2008), arXiv:0712.3009 [hep-ph]
91. Ali A, Asatrian H, Greub C. *Phys. Lett. B* 429:87 (1998), arXiv:hep-ph/9803314
92. Asatrian HM, Bieri K, Greub C, Walker M. *Phys. Rev. D* 69:074007 (2004), arXiv:hep-ph/0312063
93. Seidel D. *Phys. Rev. D* 70:094038 (2004), arXiv:hep-ph/0403185
94. Isgur N, Wise MB. *Adv. Ser. Direct. High Energy Phys.* 10:549 (1992)
95. Neubert M. *Phys. Rept.* 245:259 (1994), arXiv:hep-ph/9306320
96. Ligeti Z, Randall L, Wise MB. *Phys. Lett. B* 402:178 (1997), arXiv:hep-ph/9702322
97. Voloshin MB. *Phys. Lett. B* 397:275 (1997), arXiv:hep-ph/9612483
98. Benzke M, Lee SJ, Neubert M, Paz G. arXiv:1003.5012 [hep-ph] (2010)
99. Grant AK, Morgan AG, Nussinov S, Peccei RD. *Phys. Rev. D* 56:3151 (1997), arXiv:hep-ph/9702380
100. Buchalla G, Isidori G, Rey SJ. *Nucl. Phys. B* 511:594 (1998), arXiv:hep-ph/9705253
101. Lee SJ, Neubert M, Paz G. *Phys. Rev. D* 75:114005 (2007), arXiv:hep-ph/0609224
102. Lee KSM, Stewart IW. *Nucl. Phys. B* 721:325 (2005), arXiv:hep-ph/0409045
103. Bosch SW, Neubert M, Paz G. *JHEP* 0411:073 (2004), arXiv:hep-ph/0409115
104. Beneke M, Campanario F, Mannel T, Pecjak BD. *JHEP* 0506:071 (2005), arXiv:hep-ph/0411395
105. Chen JW, Rupak G, Savage MJ. *Phys. Lett. B* 410:285 (1997), arXiv:hep-ph/9705219
106. Buchalla G, Isidori G. *Nucl. Phys. B* 525:333 (1998), arXiv:hep-ph/9801456
107. Bauer CW, Burrell CN. *Phys. Rev. D* 62:114028 (2000), arXiv:hep-ph/9911404
108. Ligeti Z, Tackmann FJ. *Phys. Lett. B* 653:404 (2007), arXiv:0707.1694 [hep-ph]
109. Neubert M. *JHEP* 0007:022 (2000), arXiv:hep-ph/0006068
110. Bauer CW, Ligeti Z, Luke ME. *Phys. Rev. D* 64:113004 (2001), arXiv:hep-ph/0107074
111. Kruger F, Sehgal LM. *Phys. Lett. B* 380:199 (1996), arXiv:hep-ph/9603237

112. Kruger F, Sehgal LM. *Phys. Rev. D* 55:2799 (1997), arXiv:hep-ph/9608361
113. Beneke M, Buchalla G, Neubert M, Sachrajda CT. *Eur. Phys. J. C* 61:439 (2009), arXiv:0902.4446 [hep-ph]
114. Benson D, Bigi II, Uraltsev NG. *Nucl. Phys. B* 710:371 (2005), arXiv:hep-ph/0410080
115. Bosch SW, Lange BO, Neubert M, Paz G. *Nucl. Phys. B* 699:335 (2004), arXiv:hep-ph/0402094
116. Buchmuller O, Flacher H. *Phys. Rev. D* 73:073008 (2006), arXiv:hep-ph/0507253
117. Neubert M. *Eur. Phys. J. C* 40:165 (2005), arXiv:hep-ph/0408179
118. Becher T, Neubert M. *Phys. Rev. Lett.* 98:022003 (2007), arXiv:hep-ph/0610067
119. Becher T, Neubert M. *Phys. Lett. B* 633:739 (2006), arXiv:hep-ph/0512208
120. Becher T, Neubert M. *Phys. Lett. B* 637:251 (2006), arXiv:hep-ph/0603140
121. Misiak M. arXiv:0808.3134 [hep-ph] (2008)
122. Andersen JR, Gardi E. *JHEP* 0701:029 (2007), arXiv:hep-ph/0609250
123. Andersen JR, Gardi E. *JHEP* 0506:030 (2005), arXiv:hep-ph/0502159
124. Gardi E. arXiv:hep-ph/0606080 (2006)
125. Lee KSM, Stewart IW. *Phys. Rev. D* 74:014005 (2006), arXiv:hep-ph/0511334
126. Lee KSM, Ligeti Z, Stewart IW, Tackmann FJ. *Phys. Rev. D* 74:011501 (2006), arXiv:hep-ph/0512191
127. Lee KSM, Tackmann FJ. *Phys. Rev. D* 79:114021 (2009), arXiv:0812.0001 [hep-ph]
128. Poggio EC, Quinn HR, Weinberg S. *Phys. Rev. D* 13:1958 (1976)
129. Beneke M, Feldmann T. *Nucl. Phys. B* 592:3 (2001), arXiv:hep-ph/0008255
130. Beneke M, Feldmann T, Seidel D. *Nucl. Phys. B* 612:25 (2001), arXiv:hep-ph/0106067
131. Bosch SW, Buchalla G. *Nucl. Phys. B* 621:459 (2002), arXiv:hep-ph/0106081
132. Ali A, Parkhomenko AY. *Eur. Phys. J. C* 23:89 (2002), arXiv:hep-ph/0105302
133. Descotes-Genon S, Sachrajda CT. *Nucl. Phys. B* 693:103 (2004), arXiv:hep-ph/0403277
134. Ali A, Pecjak BD and C. Greub C. *Eur. Phys. J. C* 55:577 (2008), arXiv:0709.4422 [hep-ph]
135. Braun VM, Filyanov IE. *Z. Phys. C* 44:157 (1989)
136. Braun VM, Filyanov IE. *Z. Phys. C* 48:239 (1990)
137. Ball P, Braun VM, Koike Y, Tanaka K. *Nucl. Phys. B* 529:323 (1998), arXiv:hep-ph/9802299
138. Ball P, Braun VM. *Nucl. Phys. B* 543:201 (1999), arXiv:hep-ph/9810475
139. Bauer CW, Pirjol D, Stewart IW. *Phys. Rev. D* 67:071502 (2003), arXiv:hep-ph/0211069
140. Beneke M, Feldmann T. *Nucl. Phys. B* 685:249 (2004), arXiv:hep-ph/0311335
141. Lange BO, Neubert M. *Nucl. Phys. B* 690:249 (2004), arXiv:hep-ph/0311345
142. Charles J, et al. *Phys. Rev. D* 60:014001 (1999), arXiv:hep-ph/9812358
143. Becher T, Hill RJ, Neubert M. *Phys. Rev. D* 72:094017 (2005), arXiv:hep-ph/0503263

144. Feldmann T, Hurth T. *JHEP* 0411:037 (2004), arXiv:hep-ph/0408188
145. Kagan AL, Neubert M. *Phys. Lett. B* 539:227 (2002), arXiv:hep-ph/0110078
146. Becher T, Hill RJ, Neubert M. *Phys. Rev. D* 69:054017 (2004), arXiv:hep-ph/0308122
147. Arnesen CM, Ligeti Z, Rothstein IZ, Stewart IW. *Phys. Rev. D* 77:054006 (2008), arXiv:hep-ph/0607001
148. Ali A, Lunghi E, Parkhomenko AY. *Phys. Lett. B* 595:323 (2004), arXiv:hep-ph/0405075
149. Bosch SW, Buchalla G. *JHEP* 0501:035 (2005), arXiv:hep-ph/0408231
150. Beneke M, Feldmann T, Seidel D. *Eur. Phys. J. C* 41:173 (2005), arXiv:hep-ph/0412400
151. Ball P, Jones GW, Zwicky R. *Phys. Rev. D* 75:054004 (2007), arXiv:hep-ph/0612081
152. Egede U, et al. *JHEP* 0811:032 (2008), arXiv:0807.2589 [hep-ph]
153. Bobeth C, Hiller G, Piranishvili G. *JHEP* 0712:040 (2007), arXiv:0709.4174 [hep-ph]
154. Aubert B, et al. (BaBar Collab.) *Phys. Rev. Lett.* 103:211802 (2009), arXiv:0906.2177 [hep-ex]
155. Sjostrand T, Mrenna S, Skands P. *JHEP* 0605:026 (2006), arXiv:hep-ph/0603175
156. Gambino P, Giordano P. *Phys. Lett. B* 669:69 (2008), arXiv:0805.0271 [hep-ph]
157. Ciuchini M, Degrassi G, Gambino P, Giudice GF. *Nucl. Phys. B* 527:21 (1998), arXiv:hep-ph/9710335
158. Borzumati F, Greub C. *Phys. Rev. D* 58:074004 (1998), arXiv:hep-ph/9802391
159. Haisch U, Weiler A. *Phys. Rev. D* 76:034014 (2007), arXiv:hep-ph/0703064
160. Bertolini S, Borzumati F, Masiero A, Ridolfi G. *Nucl. Phys. B* 353:591 (1991)
161. Degrassi G, Gambino P, Giudice GF. *JHEP* 0012:009 (2000), arXiv:hep-ph/0009337
162. Carena MS, Garcia D, Nierste U, Wagner CEM. *Phys. Lett. B* 499:141 (2001), arXiv:hep-ph/0010003
163. Degrassi G, Gambino P, Slavich P. *Phys. Lett. B* 635:335 (2006), arXiv:hep-ph/0601135
164. Borzumati F, Greub C, Hurth T, Wyler D. *Phys. Rev. D* 62:075005 (2000), arXiv:hep-ph/9911245
165. Besmer T, Greub C, Hurth T. *Nucl. Phys. B* 609:359 (2001), arXiv:hep-ph/0105292
166. Ciuchini M, Franco E, Masiero A, Silvestrini L. *Phys. Rev. D* 67:075016 (2003), *Erratum-ibid* 68:079901 (2003), arXiv:hep-ph/0212397
167. Ciuchini M, et al. *Phys. Rev. Lett.* 92:071801 (2004), arXiv:hep-ph/0307191
168. Altmannshofer W, Guadagnoli D, Raby S, Straub DM. *Phys. Lett. B* 668:385 (2008), arXiv:0801.4363 [hep-ph]
169. Altmannshofer W, et al. *Nucl. Phys. B* 830:17 (2010), arXiv:0909.1333 [hep-ph]
170. Blanke M, et al. *Acta Phys. Polon. B* 41:657 (2010), arXiv:0906.5454 [hep-ph]
171. Ali A, Lunghi E, Greub C, Hiller G. *Phys. Rev. D* 66:034002 (2002),

- arXiv:hep-ph/0112300
172. D'Ambrosio G, Giudice GF, Isidori G, Strumia A. *Nucl. Phys. B* 645:155 (2002), arXiv:hep-ph/0207036
173. Hurth T, Isidori G, Kamenik JF, Mescia F. *Nucl. Phys. B* 808:326 (2009), arXiv:0807.5039 [hep-ph]
174. Kagan AL, Neubert M. *Phys. Rev. D* 58:094012 (1998), arXiv:hep-ph/9803368
175. Soares JM. *Nucl. Phys. B* 367:575 (1991)
176. Hurth T, Mannel T. *Phys. Lett. B* 511:196 (2001), arXiv:hep-ph/0103331
177. Hurth T, Mannel T. *AIP Conf. Proc.* 602:212 (2001), arXiv:hep-ph/0109041
178. Lee KSM, Ligeti Z, Stewart IW, Tackmann FJ. *Phys. Rev. D* 75:034016 (2007), arXiv:hep-ph/0612156
179. Gambino P, Haisch U, Misiak M. *Phys. Rev. Lett.* 94:061803 (2005), arXiv:hep-ph/0410155
180. Yan QS, Huang CS, Liao W, Zhu SH. *Phys. Rev. D* 62:094023 (2000), arXiv:hep-ph/0004262
181. Hiller G, Krüger F. *Phys. Rev. D* 69:074020 (2004), arXiv:hep-ph/0310219
182. Ball P, Zwicky R. *JHEP* 0604:046 (2006), arXiv:hep-ph/0603232
183. Grinstein B, Grossman Y, Ligeti Z, Pirjol D. *Phys. Rev. D* 71:011504 (2005), arXiv:hep-ph/0412019
184. Grinstein B, Pirjol D. *Phys. Rev. D* 73:014013 (2006), arXiv:hep-ph/0510104
185. Ball P, Zwicky R. *Phys. Lett. B* 642:478 (2006), arXiv:hep-ph/0609037
186. Feldmann T, Matias J. *JHEP* 0301:074 (2003), arXiv:hep-ph/0212158
187. Egede U, et al. arXiv:1005.0571 [hep-ph] (2010)
188. Kruger F, Sehgal LM, Sinha N, Sinha R. *Phys. Rev. D* 61:114028 (2000) *Erratum-ibid.* 63:019901 (2001), arXiv:hep-ph/9907386
189. Kruger F, Matias J. *Phys. Rev. D* 71:094009 (2005), arXiv:hep-ph/0502060
190. Altmannshofer W, et al. *JHEP* 0901:019 (2009), arXiv:0811.1214 [hep-ph]
191. Bobeth C, Hiller G, Piranishvili G. *JHEP* 0807:106 (2008), arXiv:0805.2525 [hep-ph]
192. Egede U, et al. arXiv:0912.1349 [hep-ph] (2009)
193. Chen S, et al. (CLEO Collab.) *Phys. Rev. Lett.* 87:251807 (2001), arXiv:hep-ex/0108032
194. Aubert B, et al. (BaBar Collab.) *Phys. Rev. Lett.* 97:171803 (2006), arXiv:hep-ex/0607071
195. Koppenburg P, et al. (Belle Collab.) *Phys. Rev. Lett.* 93:061803 (2004), arXiv:hep-ex/0403004
196. Limosani A, et al. (Belle Collab.) *Phys. Rev. Lett.* 103:241801 (2009), arXiv:0907.1384 [hep-ex]
197. Aubert B, et al. (BaBar Collab.) *Phys. Rev. D* 72:052004 (2005), arXiv:hep-ex/0508004
198. Aubert B, et al. (BaBar Collab.) *Phys. Rev. D* 77:051103R (2008), arXiv:0711.4889 [hep-ex]
199. Abe K, et al. (Belle Collab.) *Phys. Lett. B* 511:151 (2001), arXiv:hep-ex/0103042
200. Barberio E, et al. arXiv:0808.1297 and online update at <http://www.slac.stanford.edu/xorg/hfag> (2009)
201. Nakao M, et al. (Belle Collab.) *Phys. Rev. D* 69:112001 (2004),

- arXiv:hep-ex/0402042
202. Nishida S, et al. (Belle Collab.) *Phys. Rev. Lett.* 89:231801 (2002),  
arXiv:hep-ex/0205025
203. Aubert B, et al. (BaBar Collab.) *Phys. Rev. D* 70:091105R (2004),  
arXiv:hep-ex/0409035
204. Yang H, et al. (Belle Collab.) *Phys. Rev. Lett.* 94:111802 (2005),  
arXiv:hep-ex/0412039
205. Aubert B, et al. (BaBar Collab.) *Phys. Rev. Lett.* 98:211804 (2007),  
arXiv:hep-ex/0507031
206. Drutskoy A, et al. (Belle Collab.) *Phys. Rev. Lett.* 92:051801 (2004),  
arXiv:hep-ex/0309006
207. Aubert B, et al. (BaBar Collab.) *Phys. Rev. D* 75:051102 (2007),  
arXiv:hep-ex/0611037
208. Nishida S, et al. (Belle Collab.) *Phys. Lett. B* 610:23 (2005),  
arXiv:hep-ex/0411065
209. Aubert B, et al. (BaBar Collab.) *Phys. Rev. D* 79:011102 (2009),  
arXiv:0805.1317 [hep-ex]
210. Wedd R, et al. (Belle Collab.) arXiv:0810.0804 [hep-ex] (2008)
211. Lee YJ, et al. (Belle Collab.) *Phys. Rev. Lett.* 95:061802 (2005),  
arXiv:hep-ex/0503046
212. Nishida S, et al. (Belle Collab.) *Phys. Rev. Lett.* 93:031803 (2004),  
arXiv:hep-ex/0308038
213. Aubert B, et al. (BaBar Collab.) *Phys. Rev. Lett.* 101:171804 (2008),  
arXiv:0805.4796 [hep-ex]
214. Amsler C, et al. (Particle Data Group) *Phys. Lett. B* 667:1 (2008)
215. Atwood D, Gershon T, Hazumi M, Soni A. *Phys. Rev. D* 71:076003 (2005),  
arXiv:hep-ph/0410036
216. Ushiroda Y, et al. (Belle Collab.) *Phys. Rev. D* 74:111104R (2006),  
arXiv:hep-ex/0608017
217. Aubert B, et al. (BaBar Collab.) *Phys. Rev. D* 78:071102R (2008),  
arXiv:0807.3103 [hep-ex]
218. Li J, et al. (Belle Collab.) *Phys. Rev. Lett.* 101:251601 (2008),  
arXiv:0806.1980 [hep-ex]
219. Taniguchi N, et al. (Belle Collab.) *Phys. Rev. Lett.* 101:111801 (2008),  
arXiv:0804.4770 [hep-ex]
220. Aubert B, et al. (BaBar Collab.) *Phys. Rev. D* 78:112001 (2008),  
arXiv:0808.1379 [hep-ex]
221. Aubert B, et al. (BaBar Collab.) *Phys. Rev. Lett.* 102:161803 (2009),  
arXiv:0807.4975 [hep-ex]
222. Ushiroda Y, et al. (Belle Collab.) *Phys. Rev. Lett.* 100:021602 (2008),  
arXiv:0709.2769 [hep-ex]
223. Wei JT, et al. (Belle Collab.) *Phys. Rev. Lett.* 103:171801 (2009),  
arXiv:0904.0770 [hep-ex]
224. Aubert B, et al. (BaBar Collab.) *Phys. Rev. Lett.* 102:091803 (2009),  
arXiv:0807.4119 [hep-ex]
225. CDF Public note 10047 (2009)
226. Aubert B, et al. (BaBar Collab.) *Phys. Rev. D* 79:031102R (2009),  
arXiv:0804.4412 [hep-ex]
227. In talk given by T. Iijima at *XXIV International Symposium on Lepton  
Photon Interactions* (2009)

228. Aubert B, et al. (BaBar Collab.) *Phys. Rev. Lett.* 93:081802 (2004),  
arXiv:hep-ex/0404006

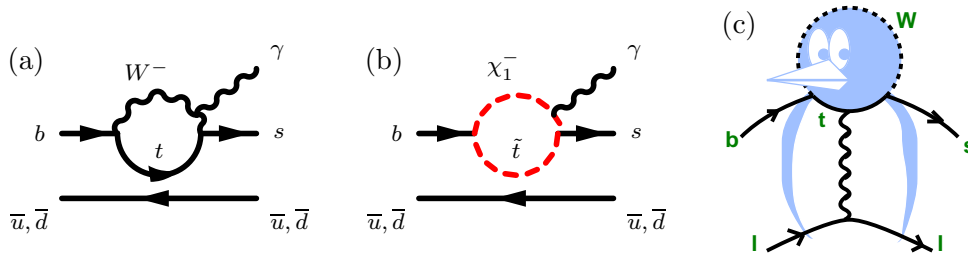


Figure 1: Examples of radiative penguin decay diagrams (a) in the Standard Model and (b) beyond. (c) A penguin.

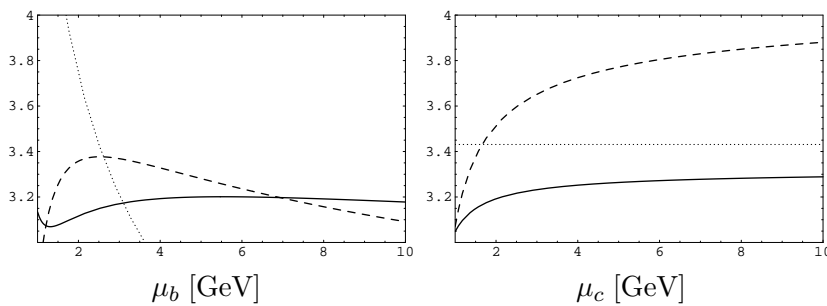


Figure 2: Renormalization-scale dependence of  $\mathcal{B}(B \rightarrow X_s \gamma)$  in units  $10^{-4}$  at leading log (dotted lines), next-to-leading log (dashed lines) and next-to-next-to-leading log (solid lines). The plots describe the dependence on (left) the the low-energy scale  $\mu_b$  and (right) the charm mass renormalization scale  $\mu_c$ , from (58).

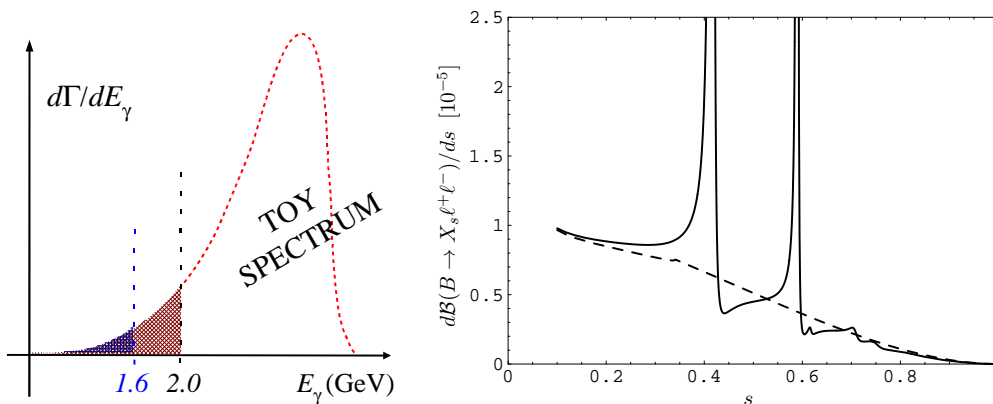


Figure 3: Spectra in inclusive modes: (left) Cut in the photon-energy spectrum in  $B \rightarrow X_s \gamma$ . (right) Differential  $B \rightarrow X_s \ell^+ \ell^-$  branching fraction as a function of  $s = q^2/m_b^2 \equiv m_{\ell^+ \ell^-}^2/m_b^2$ , including the effect of charm resonances in the Krüger-Sehgal method (solid line). For comparison, the dashed curve shows the same quantity obtained within a purely partonic calculation at next-to-leading-log precision, from Ref. (113).

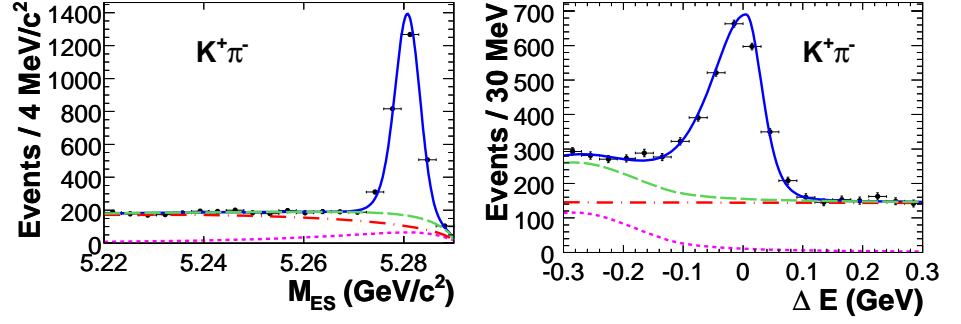


Figure 4: Example of  $M_{ES}$  ( $M_{bc}$ ) and  $\Delta E$  for  $B^0 \rightarrow K^{*0}\gamma$  by BaBar (from Ref. (154)).

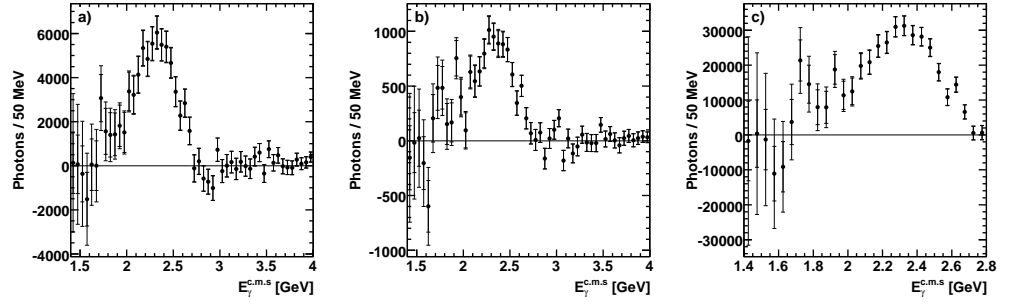


Figure 5: Photon-energy spectrum for  $B \rightarrow X_s\gamma$ , as measured by Belle (a) without lepton tag, (b) with a lepton tag, and (c) their average from Ref. (196).

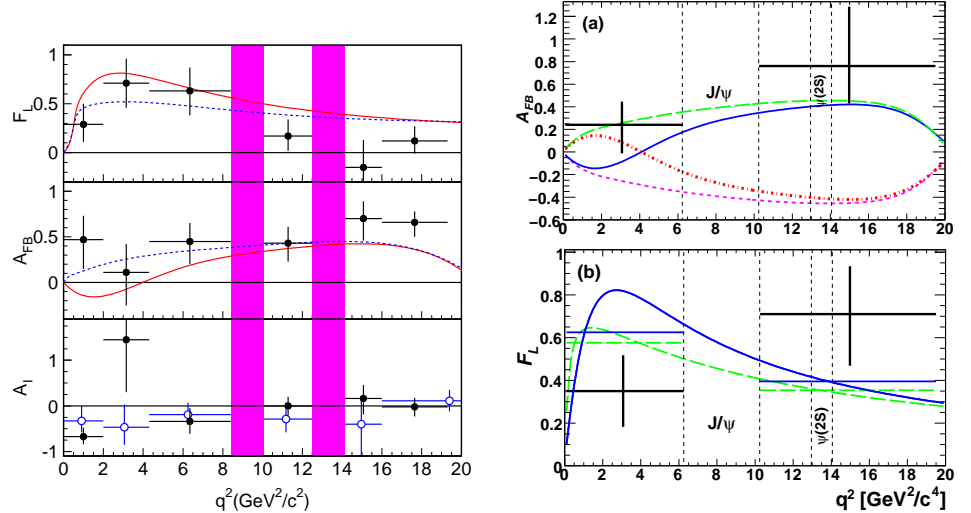


Figure 6: Longitudinal polarization fraction, forward-backward asymmetry and isospin asymmetry of  $B \rightarrow K^{*}\ell^{+}\ell^{-}$  by Belle (right, from Ref. (223)) and BaBar (left, from Ref. (226)). The solid line shows the Standard Model predictions, and the other curves represent non-Standard Model extreme cases.